Contrasting spatial and seasonal trends of methylmercury exposure pathways of Arctic seabirds: combination of large-scale tracking and stable isotopic approaches

Marina Renedo, David Amouroux, Céline Albert, Sylvain Bérail, Vegard S Bråthen, Maria Gavrilo, David Grémillet, Hálfdán H Helgason, Dariusz Jakubas, Anders Mosbech, et al.

Contrasting spatial and seasonal trends of methylmercury exposure pathways of Arctic seabirds: combination of large-scale tracking and stable isotopic approaches

Marina Renedo[1,2,*], David Amouroux[2], Céline Albert[1], Sylvain Bérail[2], Vegard S. Bråthen[3], Maria Gavrilo[4], David Grémillet[5,6], Hálfdán H. Helgason[7], Dariusz Jakubas[8], Anders Mosbech[9], Hallvard Strøm[7], Emmanuel Tessier[2] , Katarzyna Wojczulanis-Jakubas[8], Paco Bustamante[1,10], Jérôme Fort[1*]

[1] Littoral Environnement et Sociétés (LIENSs), UMR 7266 CNRS- La Rochelle Université, 2 rue Olympe de Gouges, 17000 La Rochelle, France

[2] Universite de Pau et des Pays de l'Adour, E2S UPPA, CNRS, IPREM, Institut des Sciences Analytiques et de Physico-chimie pour l'Environnement et les matériaux, Pau, France

[3] Norwegian Institute for Nature Research, Trondheim, Norway

[4] Arctic and Antarctic Research Institute, 38 Bering Street, 199397, Saint-Petersburg, Russia

[5] Centre d'Etudes Biologiques de Chizé, UMR 7372 CNRS –La Rochelle Université, 405 Route de Prissé la Charrière 79360 Villiers-en-Bois, France

[6] Percy FitzPatrick Institute, DST/NRF Centre of Excellence, University of Cape Town, Rondebosch, South Africa

[7] Norwegian Polar Institute, Tromsø, Norway

[8] Gdańsk University, Faculty of Biology, Gdańsk, Poland

[9] Aarhus University, Department of Bioscience, Roskilde, Denmark

[10] Institut Universitaire de France (IUF), 1 rue Descartes, 75005 Paris, France

**Corresponding authors:* marina.renedo@ird.fr, jerome.fort@univ-lr.fr

Abstract

Despite the limited direct anthropogenic mercury (Hg) inputs in the circumpolar Arctic, elevated concentrations of methylmercury (MeHg) are accumulated in Arctic marine biota. However, the MeHg production and bioaccumulation pathways in these ecosystems are not completely unravelled. We measured Hg concentrations and stable isotope ratios of Hg, carbon and nitrogen in feathers and blood of geolocator-tracked little auk *Alle alle* from five Arctic breeding colonies. The wide-range spatial mobility and tissue-specific Hg integration times of this planktivorous seabird allowed the exploration of their spatial (wintering quarters/breeding grounds) and seasonal (non-breeding/breeding periods) MeHg exposure. An east-to-west increase of head feather Hg concentrations (1.74-3.48 $\mu g \cdot g^{-1}$) was accompanied by significant spatial trends of Hg isotope (particularly $\Delta^{199}Hg$: 0.96 to 1.13‰) and carbon isotope ($\delta^{13}C$: -20.6 to -19.4‰) ratios. These trends suggest distinct mixing/proportion of MeHg sources between western North Atlantic and eastern Arctic regions. Higher $\Delta^{199}Hg$ values (+0.4‰) in northern colonies indicate an accumulation of more photochemically impacted MeHg, supporting shallow MeHg production and bioaccumulation in High Arctic waters. The combination of seabird tissue isotopic analysis and spatial-tracking helps tracing the MeHg sources at various spatio-temporal scales.

TOCArt- graphical abstract

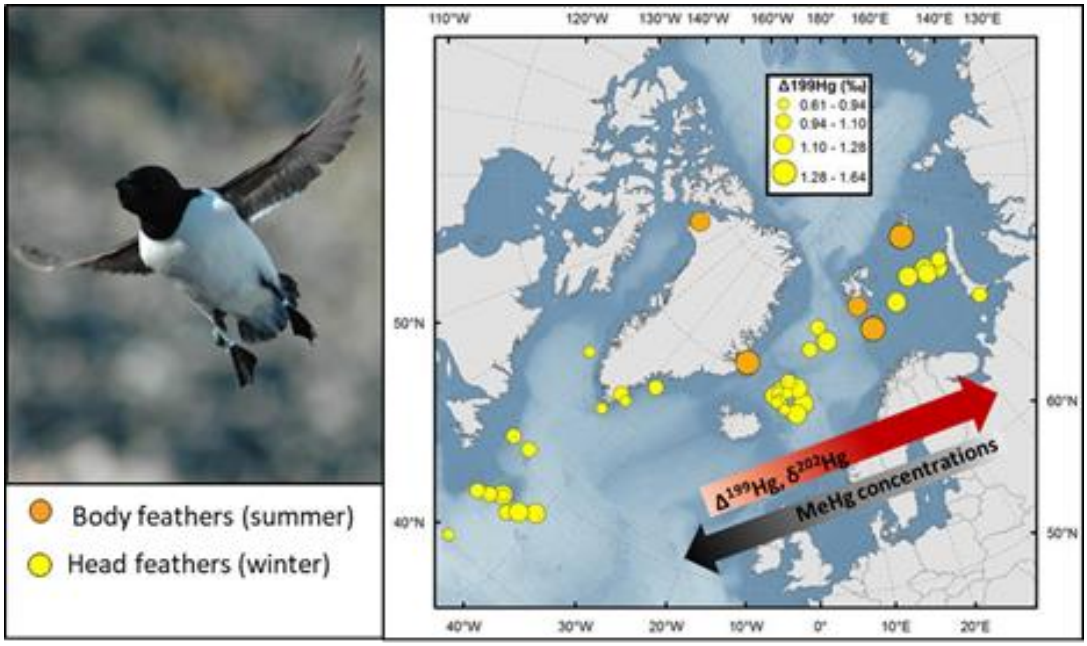

1 Introduction

Mercury (Hg) induces major risks for wildlife and human health, especially under its methylated form (methylmercury, MeHg), a potent bioaccumulative neurotoxin [1], which is mainly assimilated via fish and seafood consumption. In the ocean, MeHg production mainly occurs by biotic *in situ* methylation of inorganic Hg [2,3]. Once formed, MeHg incorporates into the food webs and biomagnifies its concentrations leading to life-impacting levels in top predators and humans. Despite little direct anthropogenic pressure in the Arctic region, Arctic ecosystems are subject to contamination by Hg transported from lower latitudes. Indeed, total Hg concentrations measured in the Arctic surface seawater are up to 2-fold higher compared to other oceanic regions [4,5]. Sea-ice melting,

direct atmospheric deposition and continental inputs originating from soil erosion and riverine circulation are considered major drivers of the high Hg levels in the Arctic [6–10]. However, the MeHg production pathways and zones in the Arctic Ocean are still not completely identified. Several studies demonstrated that Hg in Arctic marine environments may be methylated in the water column or sediments [2,11]. Potential Hg methylating bacteria were also identified in Antarctic sea ice [12]. Recent findings and modelling studies evidenced that the largest net MeHg production in Arctic water columns may occur in oxic waters at the subsurface layer (20–200 m) [6,13]. A new study also reported the high abundance of Hg methylating gens in the oxic subsurface waters of the global ocean [14], where the highest MeHg concentrations are typically observed [4]. All these findings suggest that Hg methylation in oxic waters could be a significant source of MeHg towards Arctic marine food webs. Although policy implementations for the reduction of anthropogenic Hg emissions were achieved over the last 30 years in some parts of the world, Hg levels continue to increase in biota from several regions of the Arctic [15]. Medium to high predators such as seabirds are exposed to significant environmental MeHg concentrations through their diet [15,16] and have been extensively studied as bioindicators of Hg exposure in marine food webs (e.g [17,18]), including the Arctic [19–21]. Specific foraging habitats and migratory movements of Arctic seabirds strongly determine their exposure to distinct environmental MeHg sources in marine ecosystems [22,23]. However, studies on Hg exposure in Arctic seabirds have commonly put the focus towards the breeding season (summer) when seabirds are more accessible for researchers. Consequently, the investigation of Hg exposure during the non-breeding season is still scarce due to sampling logistical difficulties.

The combination of carbon and nitrogen stable isotopes with Hg stable isotopes has demonstrated its suitability for the identification of Hg sources and the associated geochemical processes in the different marine compartments [24–26] . Therefore, its use can help understanding Hg exposure pathways of seabirds according to their migratory behaviour. Hg has seven stable isotopes (196 to 204) and fractionates dependently and independently of the isotopic masses. The combined use of Hg isotopic mass-dependent (MDF, e.g. δ^{202}Hg) and mass-independent (MIF, e.g. Δ^{199}Hg) fractionation enables the quantification of processes and the identification of sources and pathways of Hg in the environment [27], including marine ecosystems [25,26,28,29]. MDF of Hg isotopes occurs during many physical, chemical or biological processes [30–33]. However, large Hg MIF of odd isotopes (Δ^{199}Hg and Δ^{201}Hg) is observed during light-induced reactions, such as inorganic Hg photoreduction and MeHg photodemethylation. Hg MIF signature is not affected by biological or trophic processes, so it is preserved up to the food webs [34], then presenting a significant advantage to trace Hg marine sources. For instance, Arctic marine top predators reported much higher Hg odd MIF values (more photochemically impacted Hg) in non-ice covered regions, relating the importance of the accelerated melting of sea ice on the Hg polar cycle [25,35]. Also, consistent decrease of Hg odd MIF (and MDF) in pelagic fish according to their foraging depth in the North Pacific Ocean demonstrated the dilution of surface MeHg by *in situ* methylated Hg at depth [3]. More recently discovered, Hg MIF of even Hg isotopes (reported as Δ^{200}Hg) seems to occur during complex atmospheric mechanisms such as photo-oxidation in the tropopause [36]. Even-MIF is not induced during any biogeochemical nor photochemical processes in the lower troposphere or the photic zone [36–38], therefore the signature is preserved and useful to identify major potential Hg sources of atmospheric origin [10,39,40]. Due to the different

combinations of the processes involving Hg transformations in the environment, Hg isotopes fractionate differently and with different degrees of magnitude in every specific environmental compartment. Thus, the analysis of Hg stable isotopes of mobile predators such as Arctic seabirds can give access to interesting information about MeHg trophic sources at large scales of the Arctic Ocean and neighbouring water bodies.

Here we propose an original approach consisting in the combination of isotopic analyses (Hg, C and N) and wildlife tracking to provide new information about MeHg exposure pathways of seabirds at both temporal and spatial scales. For this purpose, we focused on the little auk (or dovekie, *Alle alle*), the most numerous seabird species breeding in the High Arctic (between 37 to 40 million breeding pairs estimated [41,42]). Little auks have several ecological advantages for their use as a bioindicator models. 1) They are zooplanktivorous and mainly feed on copepods belonging to two *Calanus* species (i.e., *C. glacialis* and *C. hyperboreus*) during the breeding period [43]. Therefore, they reflect MeHg accumulation in a short food chain that is strongly dependent on sea ice abundance and seawater temperature [44]. 2) They exhibit colony specific wintering areas [45], then reflecting wide-ranging spatial variability of Hg exposure [46]. 3) Little auks moult their feathers twice during their annual cycle: a partial moult (head, neck and throat feathers, hereafter 'head feathers') during the pre-breeding period (in ca. April) and a complete post-breeding moult in September [13]. During moult, seabirds excrete the Hg accumulated in their body tissues into feathers [47]. Thus, feather Hg reflects blood Hg levels at the time of feather growth which occurred at the last moulting sequence [48], then integrating Hg from current diet and/or the remobilization of Hg from tissues during moult. Thereby, the different Hg integration times between the types of feathers allow studying Hg exposure during both the non-breeding (head feathers) and the breeding (body feathers) periods in

a same individual [46]. Besides, C and N isotopic ratios of blood sampled during the breeding – chick rearing – period can provide information about summer diet and then be compared to Hg levels and isotopic composition in body feathers of little auks [49,50]. We hypothesized that variations of tissue-specific Hg isotopic signatures (body *vs* head feathers) will allow reflecting the seasonal variability (summer *vs* winter) on the Hg cycling. Besides, the exploration of both spatial grounds and isotopic information (Hg, C and N) would help tracking distinct sources of Hg contamination along with seabird migratory circulation.

2 Material and methods

2.1 Sampling sites and description of sample collection

This study was conducted during the seabird breeding seasons of 2015 and 2016 at five colonies of the Arctic Ocean: Franz Josef Land (FJL) (Hooker Island; 80.23°N, 53.01° E), Bear Island (Bjørnøya; 74.45°N, 19.04° E), East Greenland (Kap Høegh; 70.72°N, 21.55°W), Spitsbergen (Hornsund; 76.97°N, 15.78 °E) and North West Greenland (Thule; 77.47°N, 69.22° W). Blood and feathers were sampled from ten individuals per colony (n=50 for the 5 colonies). Individuals from all sites, but Thule, were equipped with a miniature geolocator data-logger (GLS, Biotrack MK4083 or Migrate Technology C65) to track their non-breeding movements and distribution, as described in previous works [45,51,52]. We treated GLS tracking data from 1st December to 30th January (period when all little auks were at their winter grounds) and calculated the median individual winter latitude and longitude for each individual separately.

2.2 Description of analytical methods

Sample preparation, analyses of total Hg and Hg species concentrations

Body and head feathers were cleaned in a 2:1 chloroform:methanol solution for 5 min in an ultrasonic bath, followed by two methanol rinses to remove surface impurities, and then oven dried at 50 °C during 48 h and homogenized to powder [46]. Since fluctuations of Hg concentrations have been observed among and within individual feathers from the same bird [53,54], we pooled a representative number of feathers of each individual (5-8 feathers) to limit the variability and provide results as accurately as possible. Blood samples were dried, lyophilized and ground to powder as described in a previous work [46]. Feather and blood total Hg concentration (hereafter expressed as $\mu g \cdot g^{-1}$, dry weight) was quantified by using an advanced Hg analyser (AMA-254, Altec).

Prior to Hg speciation analyses, blood and feathers (0.01−0.05 g) were digested following a previously developed method by microwave-assisted extraction (using a Discover SP-D microwave, CEM Corporation) [55,56]. We used 5 mL of tetramethylammonium hydroxide (25% TMAH in H2O, Sigma Aldrich) for blood samples and 5 mL nitric acid ($HNO_3 \cdot 6N$, INSTRA quality) for feather Hg extraction. The extraction was carried out in CEM Pyrex vessels by 1 min of warming up to 75 °C and 3 min at 75 °C with magnetic agitation to homogenise the samples. Quantification of Hg species was carried out by isotope dilution analysis (details in [55]), using a GC-ICP-MS Trace Ultra GC equipped with a Triplus RSH autosampler coupled to an ICP-MS XSeries II (Thermo Scientific, USA). We performed Hg speciation analyses of certified reference materials (CRM) for QA/QC purposes (Table S1). Human hair reference material (NIES-13) and feather internal reference material (F-KP, king penguin feathers) were used for validation of feather analyses (keratin-based matrixes). Blood analyses were validated with dogfish liver reference material (Dolt-5) and with internal reference material (RBC-KP, king penguins red blood cells). The reported results total Hg concentrations obtained by Hg

speciation analyses (i.e., the sum of inorganic and organic Hg) were compared to total Hg concentrations obtained by AMA-254 to verify the recovery of the extraction. Recoveries of Hg and MeHg concentrations with respect to the reference values for each material varied between 92 and 108% (Table S1).

Total Hg isotope analyses

Feather (and blood) samples (0.05−0.10 g) were digested with 3 or 5 mL of HNO_3 acid (65%, INSTRA quality) after a predigestion step overnight at room temperature. Hg extraction was carried out by Hotblock heating at 75 °C during 8 h (6 h in HNO_3 and 2 h more after addition of 1/3 of the total volume of H_2O_2 30%, ULTREX quality). The digest mixtures were finally diluted in an acidic matrix (10% HNO_3 and 2% HCl) with final Hg concentrations ranging from 0.5 to 1 ng·mL^{-1}. Hg isotopic composition was determined using cold-vapor generator (CVG)-MC-ICPMS (Nu Instruments), detailed in previous work [56]. Hg isotopic values were reported as delta notation, calculated relative to the bracketing standard NIST SRM-3133 reference material to allow interlaboratory comparisons, as described in the SI. NIST SRM-997 thallium standard solution was used for the instrumental mass-bias correction using the exponential law. Secondary standard NIST RM-8160 (previously UM-Almadén standard) was used for validation of the analytical session (Table S2).

Recoveries of extraction were verified for all samples by checking the signal intensity obtained on the MC-ICPMS for diluted extracts relative to NIST 3133 standard (with an approximate uncertainty of ±15%). Total Hg concentrations in the extract solution were compared to the concentrations found by AMA-254 analyses to assess method recovery. Total Hg concentrations in the extract solution were compared to the concentrations found

by AMA-254 analyses to assess method recovery. Average recoveries obtained were 98 ± 14% for feathers (n = 104) and 100 ± 2% for blood samples (n = 102). Accuracy of Hg isotopic analyses for keratin matrixes was evaluated with validated human hair material NIES-13 isotopic composition [57]. Hg isotopic results for blood samples were validated with reference values of Lake Michigan fish tissue NIST SRM 1947. Internal reference samples of feathers (F-KP) and avian blood (RBC-KP) were also measured. Uncertainty for delta values was calculated using 2SD typical errors for each internal reference material (Table S2).

Carbon and nitrogen stable isotope analyses

Homogenized feather and blood subsamples (aliquots mass: ~0.3 mg) were weighed with a microbalance and packed in tin containers. Carbon ($\delta^{13}C$) and nitrogen ($\delta^{15}N$) stable isotope ratios were determined with a continuous flow mass spectrometer (Thermo Scientific Delta V Advantage) coupled to an elemental analyser (Thermo Scientific Flash EA 1112). Results are in delta notation relative to Vienna PeeDee Belemnite and atmospheric N_2 for $\delta^{13}C$ and $\delta^{15}N$, respectively. Replicate measurements of internal laboratory standards (acetanilide) indicated measurement errors < 0.15‰ for both $\delta^{13}C$ and $\delta^{15}N$ values. USGS-61 and USGS-62 reference materials were also analysed for calibration.

2.3 Statistical analyses

Statistical analyses were performed using the software R 3.3.2 (R Core Team, 2018) [58]. Before statistical analyses, the data were checked for normality of distribution and homogeneity of variances using Shapiro–Wilk and Breusch-Pagan tests, respectively. Since data did not meet specificities of normality and homoscedasticity, non-parametrical

tests (Kruskal–Wallis with Conover-Iman *post-hoc* test) were performed. Statistically significant results were set at $\alpha = 0.05$. Statistical significance of Hg concentration and isotopic differences between head and body feathers were assessed using a randomization procedure. A 99% confidence interval was calculated by means of bootstrap estimation method (n=1000 iterations).

We examined the correlations between Hg concentrations, $\delta^{13}C$, Hg MDF ($\delta^{202}Hg$) and MIF ($\Delta^{199}Hg$ and $\Delta^{200}Hg$), latitude and longitude using linear regressions and Spearman correlation rank tests. The influence of the latitude and longitude of their individual breeding and non-breeding distribution on feather Hg isotopic signatures were tested using linear mixed models (LMMs) with colonies as random effect on the whole data set, using the R package "lme4" [59]. Summer latitude, summer longitude and both summer latitude + longitude together were used as predictors for Hg isotopic signatures of body feathers. Similarly, median winter latitude, median winter longitude and both median together were used as predictors of Hg isotopic signatures in head feathers. Variance inflation factors were always < 3 [60], ensuring that there was not collinearity between latitude and longitude in summer (breeding colonies) and median latitude and longitude in winter (wintering areas) [61]. The different models were ranked based on Akaïke's Information Criteria adjusted for small sample sizes (AICc) and compared using ΔAICc and Akaike weights (w) using the R package "wiqid" [62]. To assess the explanative power of these models, marginal R^2 was obtained using the R package "r2glmm" [63].

3 Results and discussion

3.1 Seasonal and geographical variations of feather MeHg concentrations related to changing foraging habits ($\delta^{15}N$)

We observed that the dominant fraction of Hg was in the form of MeHg both in body feathers and blood (94 ± 2%, n=20 and 90 ± 3%, n=10; respectively) for all the studied populations of little auks (Table S3). This result is in good agreement with previous studies [55,56,64,65] and supports that both tissues of little auks principally present Hg as MeHg. Body and head feathers are known to be grown at different times and therefore the Hg excreted in head and body feathers reflects respectively the exposure during their wintering (October to April) and breeding (May to September) periods. Since birds are known to excrete between 70 and 90% of their Hg body burden by feather moult [48], we cannot exclude that some residual Hg accumulated during the non-breeding period could also be excreted during body feather moult, and vice versa, but this fraction would be minor.

Overall, individuals presented higher Hg (MeHg) concentrations in head compared to body feathers, exhibiting up to 2-fold higher concentrations in head feathers in the case of East Greenland and Bear Island populations (Table S4). Higher Hg concentrations of head feathers are coherent with previous observations [22] and suggest a higher exposure to MeHg during the non-breeding period outside the High Arctic. For instance, little auks breeding in areas of Spitsbergen and East Greenland are known to mainly forage on copepods (*Calanus* spp.) during the breeding season [43]. However, the seasonal vertical migration of their main prey *Calanus* spp. to inaccessible depths produces a seasonal shift in their diet towards krill *Meganyctiphanes norvegica*, hyperiid amphipods *Themisto* spp.,

and fish larvae [66]. The consumption of higher trophic level prey during winter could explain the higher Hg levels excreted during the spring moult (head feathers), whereas they are probably less exposed to Hg in summer.

We also observed high variations of Hg concentrations in head feathers among individuals of the same colony, especially in Bear Island (from 0.81 to 4.35 µg g^{-1}) and Spitsbergen populations (from 1.67 to 3.79 µg g^{-1}) (Fig. S1). This could be due to the wide-spread individual foraging specialisation during their non-breeding period and the consumption of a wider range of prey [67]. Conversely, little auks occupy more restricted foraging areas during the breeding season due to the need to frequently feed their chicks and therefore feed on local prey captured near their respective colonies [68], leading to less intra-population variability of Hg concentrations in their body feathers.

We observed a consistent longitudinal trend of body feather Hg concentrations (R^2=0.58, p<0.0001) with increasing Hg levels from eastern (Bear Island and FJL, 0.71 and 0.75 µg·g^{-1}, respectively) to western colonies (NW Greenland, 2.07 µg·g^{-1}) (Figure 1). When applying mixed models, summer longitude was the most supported predictor of body feather Hg concentrations (Table S6). Head feather Hg concentrations were positively correlated both with winter latitude and longitude for the four spatially tracked populations (R^2=0.54 and R^2=0.60, respectively; both p<0.0001) (Figure 1). Both variables together were considered as predictors of Hg head feather concentrations by linear mixed models (Table S7). Head feather concentrations were higher in populations wintering in western zones (3.48 µg·g^{-1}, East Greenland population) and decreased gradually and significantly (H=20.13, p=0.001) in those wintering in northeast areas (1.74 µg·g^{-1}, FJL population). The consistent longitudinal patterns both in summer and winter

reflect a higher accumulation of MeHg in little auks from western regions, whereas colonies breeding in Arctic northern regions seem to be exposed to lower concentrations.

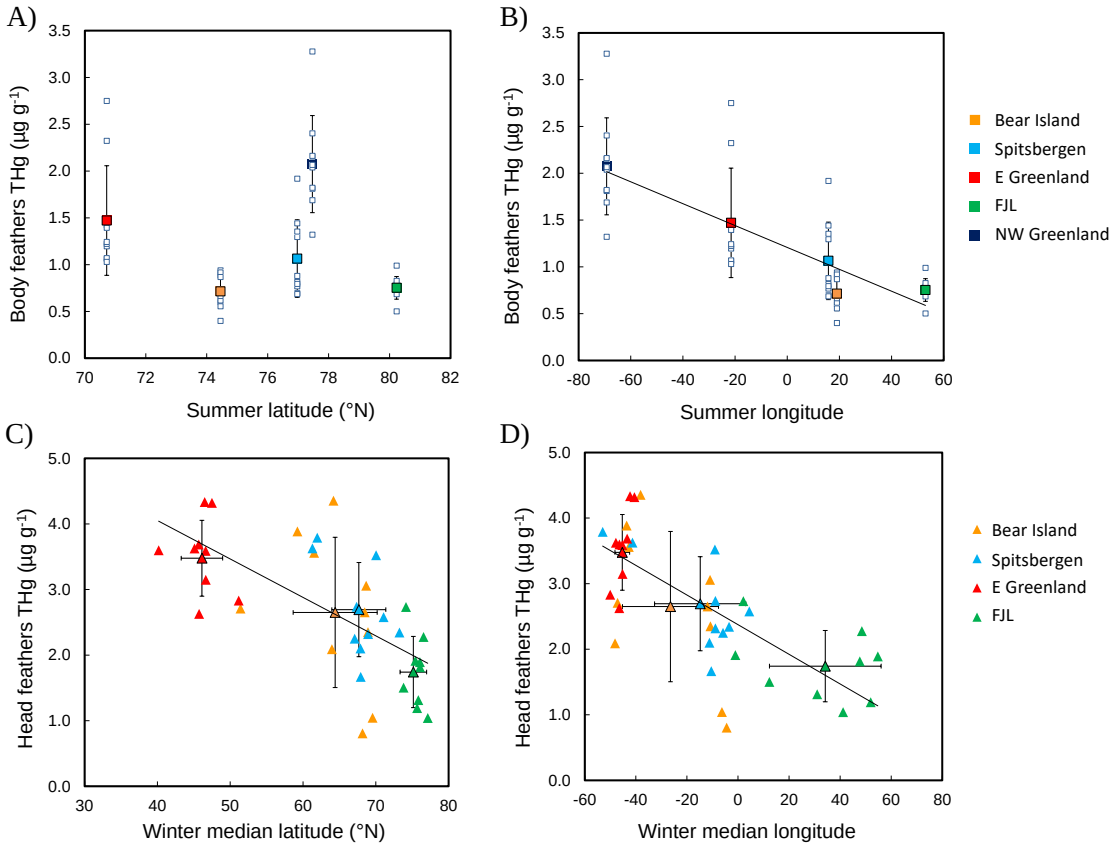

Figure 1. Hg concentration (µg·g^{-1}) of little auk body feathers (summer) as a function of latitude (A) and longitude of their breeding sites (B) and head feathers (winter) as a function of the median latitude (C) and longitude (D) of their winter grounds. Regression lines are A) Slope: 0.052±0.013, intercept: -3.420±0.997, R^2=0.26, p=0.005; B) Slope: -0.012±0.001, intercept: 1.209±0.059, R^2=0.58, p<0.0001; C) Slope: -0.059±0.011, intercept: 6.399±0.669, R^2=0.54, p<0.0001; D) Slope: -0.022±0.003, intercept: 2.375±0.120, R^2=0.60, p<0.0001. Regression lines presented only for significant relationship between the two variables.

Seabird blood $\delta^{15}N$ values provide short- to medium-term information (about 1–5 weeks) while feathers $\delta^{15}N$ values reflect the diet at the time they were grown [50,69]. The distribution of little auk populations in winter was limited to the North Atlantic and the

Arctic areas, where large-scale $\delta^{15}N$ values are known to be relatively homogeneous at the base of the food web [70,71], then allowing the inter-population comparison. The lower body feather Hg concentrations and blood $\delta^{15}N$ values observed in little auks (Table S5) suggest that all birds from the different populations mostly feed at low trophic levels and on *Calanus* copepods in summer. Contrarily, the interpopulation differences of $\delta^{15}N$ values in winter (head feathers) were much more pronounced (Table S4). For instance, little auk populations breeding in FJL and Bear Island exhibited a ~3 ‰ higher $\delta^{15}N$ values in head feathers than in blood. This difference highlights the spatial variability of $\delta^{15}N$ values in relation to the different winter distribution of little auks in winter. Previous studies have reported significant seasonal variations in copepod $\delta^{15}N$ values (up to 6‰) between late winter and spring (highly productive periods) relative to the summer and autumn periods [71,72]. The seasonal variability of zooplankton $\delta^{15}N$ values is common on the eastern and western parts of the North Atlantic Ocean and needs to be considered here due to the wide spatial distribution of little auks in winter. Therefore, the higher feather Hg concentrations little auk colonies from western parts of the Arctic Ocean could be influenced by their seasonal dietary shifts and different spatial distribution but also by the complex Hg oceanic dynamics or distinct environmental sources that control the level of exposure to MeHg at the different regions.

3.2 Spatio-temporal trends of Hg MDF ($\delta^{202}Hg$) in feathers related to ecological aspects

Specific Hg integration times of seabird tissues may influence the seasonal incorporation of MeHg from different spatial origin [73]. However, the geographical variations in $\delta^{202}Hg$ values are generally difficult to distinguish since metabolic processes also induce Hg MDF. Head and body feathers showed large ranges of $\delta^{202}Hg$ values, varying from -0.24 to 1.43 ‰ and from -0.11 to 1.28 ‰, respectively. Although we focused on the study of

multiple colonies of the same seabird species to minimize the metabolic or trophic-related effects, we cannot exclude that the variability of δ^{202}Hg signatures among colonies is led only by the specific isotopic baseline of their respective foraging habitats. For instance, FJL population exhibited significantly heavier δ^{202}Hg values relative to the other four populations, both in head ($H=29.42$, $p<0.0001$) and body feathers ($H=27.69$, $p<0.0001$) (Table S4). It is known that little auks from FJL are morphologically bigger than those of the populations from Svalbard due to more severe climate conditions in this area [74]. Thus, potentially different morphological characteristics associated to their bigger size could contribute to higher feather δ^{202}Hg values in this colony. Hg concentrations and δ^{202}Hg values of head feathers were highly correlated for the overall populations ($R^2=0.52$, $p<0.0001$), while Δ^{199}Hg signatures were not related to Hg concentration in any type of feather (Figure S2). This observation shows the completely decoupled behavior between δ^{202}Hg and Δ^{199}Hg signatures. The influence of biological and ecological factors on δ^{202}Hg values shows the limitation of this type of signature to discern spatial MeHg sources related to different migratory routes of seabird populations. The utilisation of feather δ^{202}Hg values as a proxy of geographical patterns or to changing environmental conditions requires a complete knowledge of all the processes and factors driving Hg MDF (i.e., trophic ecology and intrinsic metabolic/physiological processes).

3.3 Hg odd-MIF (Δ^{199}Hg): seasonal and spatial differences of Hg marine photochemistry

Head and body feather odd-MIF values (Δ^{199}Hg) ranged from 0.72 to 1.26 ‰ and 0.90 to 1.91 ‰, respectively. Significantly higher Δ^{199}Hg values in body compared to head feathers (Table S8) suggest a seasonal variability in odd-MIF values. This could be primarily associated to the vertical migration of little auk main prey (copepods) and the

consequent seasonal shift on their diet to krill/amphipods during the winter season. Their seasonal diet shift could enhance the accumulation of pelagic MeHg that is less connected to the photic zone during winter, then leading to lower Δ^{199}Hg values of the MeHg excreted into head feathers. A previous study on subantarctic penguins documented significant differences of Δ^{199}Hg values as a function of their specific foraging depths [24], increasing around 0.4 ‰ from benthic to epipelagic populations. Although the little auk populations studied here are known to mainly feed on the same prey items and forage at similar depths, we should consider that changes on the availability of their prey among sites could also contribute to different feather Δ^{199}Hg values among populations. Further, due to the diurnal migration of zooplankton from deep water to the surface, the mixed pool of Hg accumulated in these organisms originate from different depths of the water column and therefore, their Δ^{199}Hg values represent a mixture from deep (low photodemethylated) Hg and surface Hg uptake [75]. Together with the trophic and ecological factors, we could expect that the seasonal variability of feather Δ^{199}Hg values (body *vs* head feathers) of little auks could be also influenced by a higher extent of Hg marine photochemistry occurring during summer. In summertime/ spring, little auks are known to return to their breeding sites, located at northern latitudes, where they are exposed to longer daily photoperiod at this moment of the year (polar day). Nevertheless, the weak differences of Δ^{199}Hg values between body and head feathers of a same population (from 0.26 to 0.50 ‰, Table S8) seem to indicate low variations of MeHg photodemethylation extents between their summer and winter sites. Therefore, the differences on daily photoperiod and/or light penetration between their summer and wintering foraging grounds would have a minor role on Hg isotopic variations.

Concerning the spatial variability of Δ^{199}Hg values among colonies, we observed positive linear relationships between body feather Δ^{199}Hg values and summer longitude (R^2=0.20, p<0.0001) and between head feather Δ^{199}Hg values and winter longitude (R^2=0.22, p<0.0001) (Figure 2). Summer and winter longitudes were respectively the most supported explanatory factors of body and head feather Δ^{199}Hg values (Tables S6 and S7). No significant relationships were observed with latitude in summer (R^2=0.01, p=0.20) nor winter (R^2=0.07, p=0.06) (Figure 2). FJL population, the northern colony of this study, showed slightly higher body feather Δ^{199}Hg values (1.64 ± 0.15 ‰, n=10, 80ºN) comparing to other studied colonies (1.31 ± 0.20 ‰, n=37 70-77ºN) (H=11.96, p=0.018). FJL individuals also presented higher Δ^{199}Hg values of their head feathers (1.13 ± 0.06 ‰) compared to the other colonies (1.00 ± 0.12 ‰) (H=18.55, p=0.001). Previous studies on Alaskan seabirds reported around 2-fold higher mean Δ^{199}Hg signatures in low-ice-covered oceanic areas (1.13 ± 0.16 ‰; 56-58ºN) than highly ice-covered regions (0.53 ± 0.15 ‰; 68ºN) and revealed that the presence of sea ice inhibits light penetration and therefore, Hg marine photochemistry [25]. Compared to the latitudinal trend observed in Alaska, the spatial variations of Δ^{199}Hg values between northern and southern populations of little auks are relatively weak and, interestingly, presented an inversed tendency between highly ice-covered (FJL) and non-ice-covered areas (North Atlantic regions). Therefore, we cannot presume that the presence of sea ice is a driving factor controlling MeHg photochemistry and the related odd-MIF signatures registered in feathers of little auks. The existence of an opposed north-to-south trend of Δ^{199}Hg values between the Eastern and Western Arctic Ocean regions reveals different Hg dynamic systems, especially for Hg accumulation pathways in food webs.

According to previous findings, the largest MeHg production in the Arctic water column seems to occur in oxic surface waters just below the productive surface layer [6,13]. In the Arctic, additional sources of Hg and carbon are provided by sea ice algae during spring blooms [76]. The presence of terrestrial organic matter and sea ice layers that concentrates phytoplankton near the MeHg production zone may favour the Hg microbial methylation at shallow depths of the Arctic water column [12,77]. Shallower methylation occurring in Arctic waters may result in higher photochemical impact on MeHg before its assimilation in Arctic biota compared to North Atlantic marine food webs. This phenomenon could contribute to the higher feather Δ^{199}Hg values of FJL little auks compared to populations breeding at lower latitudes. The slight differences of Δ^{199}Hg values between northern and southern colonies of little auks are similar to the ranges recently observed in seabirds covering a wider latitudinal gradient (37 to 66°S) in the Southern Ocean, for which Δ^{199}Hg values increased from Antarctic (1.31 to 1.73 ‰) to subtropical (1.69 to 2.04 ‰) populations [78]. The slight variations of Δ^{199}Hg values also found between these distant sites of the Southern Ocean were translated into low differences of MeHg photochemical demethylation extents among sites and a dominance of MeHg with a mesopelagic origin in these remote environments. As previously discussed, the vertical daily migration of copepods from deep water to the surface leads to the integration of Hg from relatively deep zones of the water column therefore, contributing to the incorporation of low photochemically impacted Hg in consumers [75]. Therefore, although the planktivourous little auk feed at surface waters on the photic zone, their relatively low feather Δ^{199}Hg values suggest that the Hg accumulated in their main prey could originate from Hg pools from deeper zones of the water column.

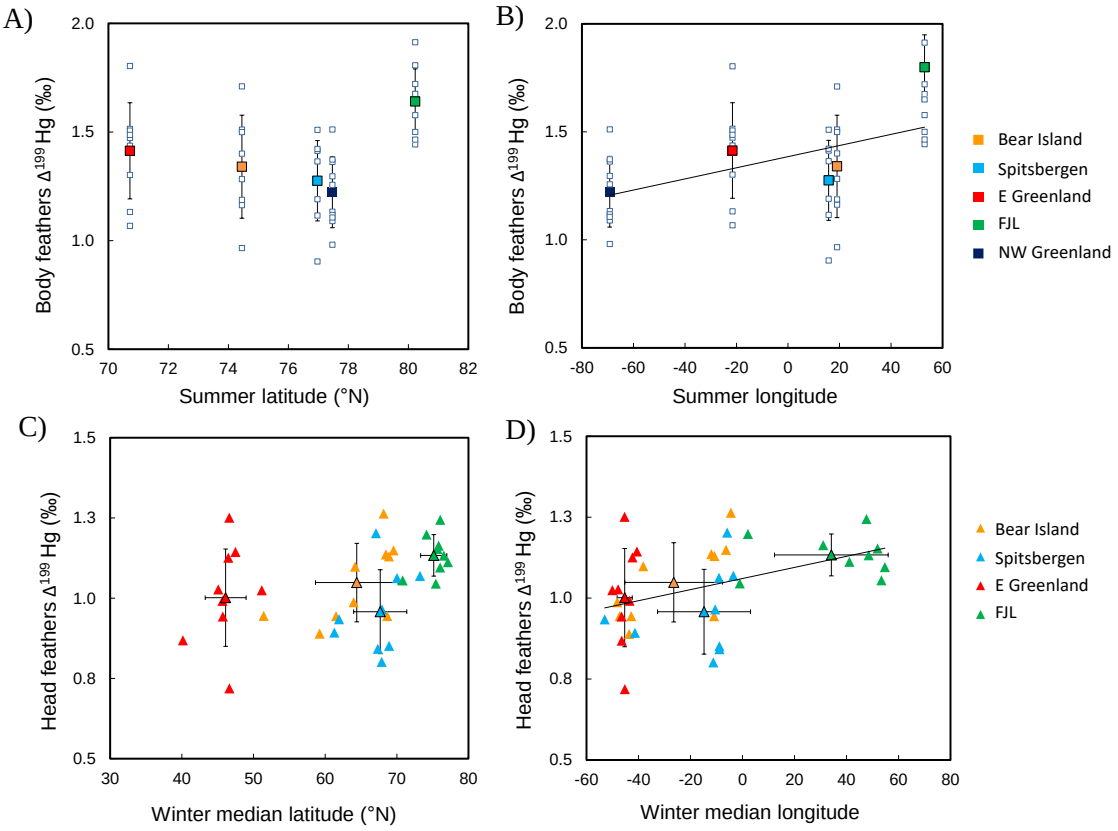

Figure 2. Hg odd-MIF (Δ^{199}Hg) of little auk body feathers (summer) as a function of latitude (A) and longitude of their breeding sites (B) and head feathers (winter) as a function of the median latitude (C) and longitude (D) of their wintering grounds. Regression lines are A) Slope: 0.014±0.011, intercept: 0.319±0.822; R^2=0.01, p=0.20; B) Slope: 0.002±0.001, intercept: 1.384±0.031, R^2=0.20, p<0.0001; C) Slope: 0.004±0.002, intercept: 0.784±0.123, R^2=0.07, p=0.06; D) Slope: 0.001±0.001, intercept: 1.069±0.022, R^2=0.22, p=0.002. Regression lines presented only for significant relationship between the two variables.

3.4 Spatial correlation of Hg MIF signatures and carbon stable isotopes (δ^{13}C)

The deposition of atmospheric Hg from mid-latitude anthropogenic emissions into the Arctic Ocean could contribute to the accumulation of MeHg from distinct origin in Arctic-North Atlantic food webs [7]. Although body feathers of little auk presented a relative high range of Δ^{200}Hg signatures (from -0.23 to 0.17 ‰), the inter-population differences were not significant (H=3.685, p=0.45) (Figure S5). No substantial interpopulation variations

of Δ^{200}Hg values were neither observed for head feathers of little auks (-0.14 to 0.12 ‰), therefore we cannot discriminate Hg sources from distinct atmospheric origin among seabird wintering grounds. Nevertheless, the spatial trends of Δ^{200}Hg values observed in little auks are more variable than those previously reported on Arctic marine mammals and seabirds of Alaska (from −0.01 to 0.10 ‰; 71 to 54 °N [79]) and on Antarctic and subtropical seabirds (from −0.02 to 0.04 ‰, 66 to 37 °S [78]).

Large-scale ocean circulation and vertical transport processes throughout the water column could influence the distribution of distinct MeHg sources between the widely distributed compartments used by little auks. The exploration of carbon stable isotopes (δ^{13}C) of little auks could help discriminating the potential contributions of distinct MeHg sources linked to the widely specific foraging habitats of little auks. Contrary to Hg isotopes, body feather δ^{13}C values do not reflect the period of summer but the moult period in late summer/early autumn (September) when they are grown [45]. To ensure only the integration of the summer, breeding period, we compared body feather Hg isotopes with blood δ^{13}C values. Little auks from FJL exhibited the lowest blood δ^{13}C values (-23.13 ± 0.84 ‰) and NW Greenland individuals the highest (-20.07 ± 0.35 ‰) relative to the rest of the colonies ($H=40.74$, $p<0.0001$) (Table S5). Head feather δ^{13}C values separated little auk populations in those overwintering in western areas of the North Atlantic Ocean and those wintering in north-eastern areas ($H=26.28$, $p<0.0001$). The gradient of δ^{13}C values of head feathers increased from populations of FJL (-20.59 ± 0.40 ‰) and Bear Island (-20.35 ± 0.38 ‰), to Northwest (-19.41 ± 0.57 ‰) and East Greenland (-19.61 ± 0.46 ‰) populations. Latitudinal gradients of δ^{13}C values of the dissolved inorganic carbon are commonly observed in surface waters as an influence of the physical and biological processes [71]. For instance, it is known that CO_2 solubility is

favoured in cold oceanic waters and consequently, surface waters at high latitudes have relatively low $\delta^{13}C$ values due to the introduction of isotopically light atmospheric CO_2. By contrast, surface waters of outgassing upwelling equatorial areas become enriched on $\delta^{13}C$ values [80,81]. Parallelly, the $\delta^{13}C$ values of primary producers are strongly influenced by the $\delta^{13}C$ values of dissolved inorganic carbon and therefore, by the temperature gradients and CO_2 solubility [71]. Spatial gradients of sea surface temperature and CO_2 concentrations could thus explain the more depleted $\delta^{13}C$ baseline in cold high Arctic marine food webs and the enrichment in $\delta^{13}C$ values when going southward to North Atlantic oceanic areas. Furthermore, the dominance of distinct marine currents between the different wintering seabird sites could strongly determine the $\delta^{13}C$ at the base of the food webs. The FJL archipelago and surrounding high Arctic areas are strongly impacted by the Makarov and Arctic cold currents flowing southward from the north, and potentially contributing to transport isotopically depleted carbon from high latitude areas. In contrast, little auk wintering regions near the Newfoundland Island (East and West Greenland populations) are affected by the Gulf Stream and North Atlantic Current [45] which could supply carbon organic matter from warmer water masses [82].

Significant negative linear relationships were obtained between $\Delta^{199}Hg$ and $\delta^{13}C$ values both in summer (R^2=0.17, p=0.003) and winter (R^2=0.31, p<0.0001) (Figure 3). Interestingly, the negative relationship between $\Delta^{199}Hg$ and $\delta^{13}C$ values of little auks contrasts with those previously reported on eggs from guillemot species (or murres, *Uria aalge* and *U. lomvia*) breeding in the Alaskan Arctic [26]. These authors reported a co-enrichment of egg $\delta^{13}C$ and $\Delta^{199}Hg$ values linked to the transition from terrestrial to marine Hg sources and the subsequent reduction of Hg photochemistry in coastal reservoirs due to higher turbidity [26]. However, the wintering areas of little auks mainly

correspond to more opened oceanic areas as the study in the Bering Sea and probably do not present such a remarkable coastal-oceanic gradient. The significant correlation obtained here between Δ^{199}Hg and δ^{13}C signatures both in body and head feathers of little auks reflect common spatial trends summer and winter foraging grounds. This interesting relationship seems be associated to both the spatial gradient of physical parameters controlling C isotopic baselines (temperature and CO_2 exchange in surface waters) and to the extent of Hg photochemical processes. Probably, a higher stratification and impact of sea ice cover in high Arctic oceanic zones favours the methylation of Hg in surface waters [13], and the extent of photochemical reactions leading to slightly positive Δ^{199}Hg values and more negative δ^{13}C values of biota. The dominance of northern marine currents in this area would also contribute to depleted δ^{13}C values. Although we could consider the existence of distinct carbon inputs transported by the marine currents on these ecosystems (i.e. external carbon supply, planktonic production), the complex interaction of oceanographic and physical parameters governing these areas does not allow to provide conclusive evidence from our data.

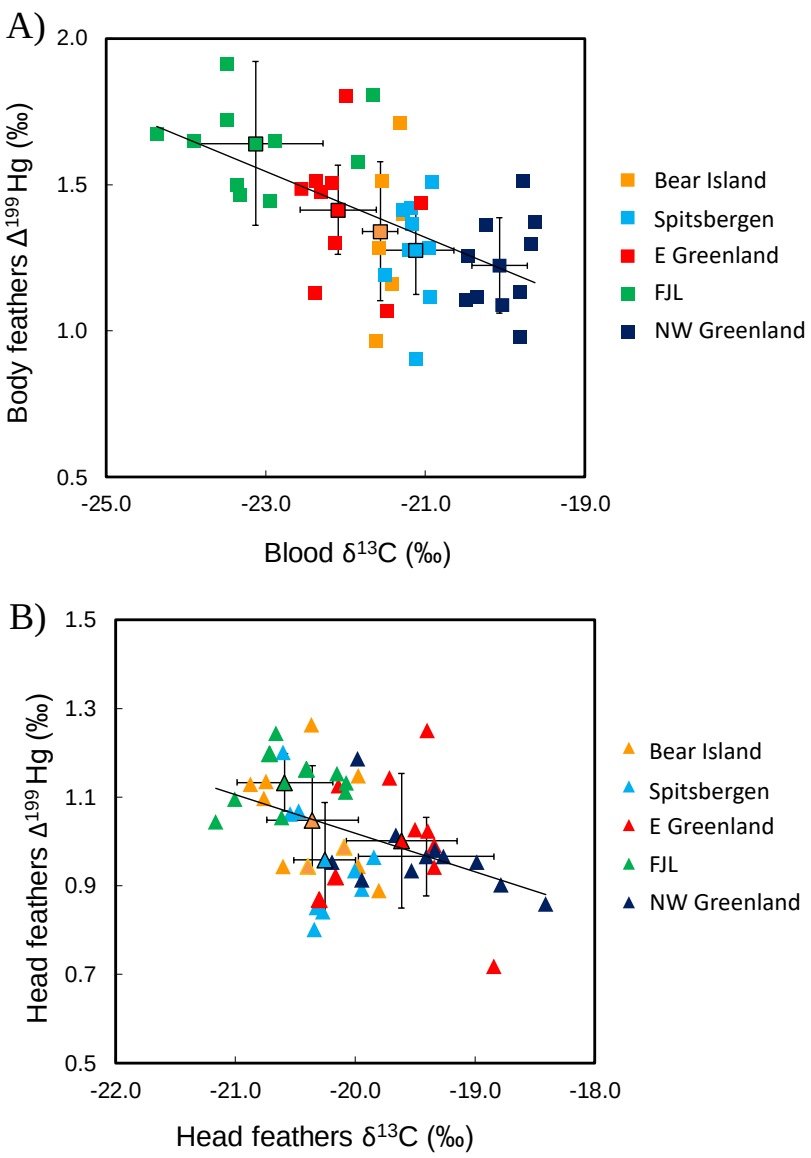

Figure 3. Carbon ($\delta^{13}C$) vs MIF Hg signatures for A) summer (body feathers) and B) winter (head feathers) periods. Regression lines are A) Slope: -0.122±0.026, intercept: -1.045±0.558, R^2=0.31, p<0.0001; B) Slope: -0.088±0.028, intercept: -0.746±0.566, R^2=0.17, p=0.003.

3.5 Geographically distinct Hg source mixing across the Arctic and North Atlantic Oceans

Our results suggest that the variations in relation to longitude of the Hg concentrations, Δ^{199}Hg, and δ^{13}C values of little auks is linked to the assimilation of isotopically distinct MeHg depending on their wintering grounds. Figure 4 shows a compilation of Hg odd-MIF values observed in little auks compared to previous studies in Arctic biota over a wide spatial scale. The observed isotopic spatial variability across the different regions of the Arctic Ocean suggests the existence of two different Hg systems between East (Atlantic) and West (Pacific) Arctic Ocean regions. Our opposed trend of Δ^{199}Hg from north to south populations values relative to Western Arctic compartments [25,35] indicates that the presence of sea ice cover is not the only driving factor controlling Hg photochemistry in the Eastern Arctic Ocean. Possibly, an additional supply of Hg and carbon sources by sea-ice algae may enhance the microbial/photochemical methylation and demethylation processes at shallower depths [6,13] in East Arctic regions, therefore contributing to the higher odd-MIF values of Hg accumulated in biota. The inversed relationship of Δ^{199}Hg and Δ^{200}Hg values of little auks with latitude is opposed to the latitudinal covariation of Δ^{199}Hg and Δ^{200}Hg in biota from Western Arctic regions [79] and from Antarctic regions [78] and evidences a completely different functioning of Hg cycling compared to other polar marine environments. Complex Hg dynamics and ocean control factors seem to drive the increasing pattern of Hg isotopes from west to east regions of the Arctic Ocean. Future research assessing large scale and long-term Hg contamination are necessary to have a complete understanding of the Hg exposure pathways and of the associated risks for the whole marine Arctic environments.

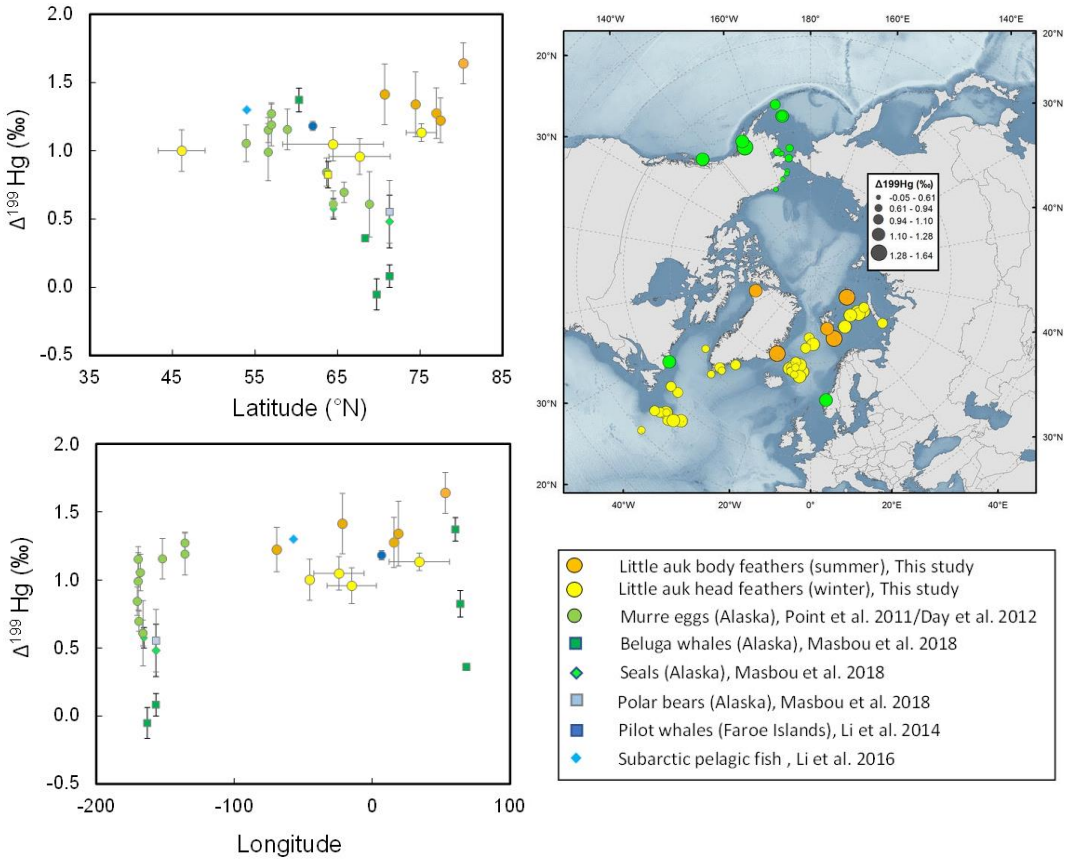

Figure 4. Compilation of Hg odd-MIF values (Δ^{199}Hg) of marine biota from spatially distant Arctic Regions. The map comprises both little auk breeding sites (orange), individual little auk median winter positions (yellow) and previous published data (green) including seabirds [25,26], beluga whale, seals and polar bears [79] from Alaskan Regions; pilot whales from Faroe Islands [28], and fish from the Labrador Sea [83].

Acknowledgements

The authors wish to thank the fieldworkers who collected the samples. Field procedures were authorized by the Ethics Committee of Institut Polaire Français Paul Emile Victor (IPEV) and by the Comité de l'Environnement Polaire. This study received financial and logistical support from the French Agency for National Research (ANR MAMBA project ANR-16-TERC-0004, ILETOP project ANR-16-CE34-0005), the French Arctic

Initiative - CNRS (PARCS project), the Mission pour l'Interdisciplinarité - CNRS (Changements en Sibérie project) and the French Polar Institute (IPEV - Pgr 388 ADACLIM). The IUF (Institut Universitaire de France) is also acknowledged for its support to PB as a senior member.

References

(1) Tan, S. W.; Meiller, J. C.; Mahaffey, K. R. The Endocrine Effects of Mercury in Humans and Wildlife. *Crit. Rev. Toxicol.* **2009**, *39* (3), 228–269. https://doi.org/10.1080/10408440802233259.

(2) Lehnherr, I.; St. Louis, V. L.; Hintelmann, H.; Kirk, J. L. Methylation of Inorganic Mercury in Polar Marine Waters. *Nat. Geosci.* **2011**, *4* (April), 298–302. https://doi.org/10.1038/ngeo1134.

(3) Blum, J. D.; Popp, B. N.; Drazen, J. C.; Anela Choy, C.; Johnson, M. W. Methylmercury Production below the Mixed Layer in the North Pacific Ocean. *Nat. Geosci.* **2013**, *6* (10), 879–884. https://doi.org/10.1038/ngeo1918.

(4) Mason, R. P.; Choi, A. L.; Fitzgerald, W. F.; Hammerschmidt, C. R.; Lamborg, C. H.; Soerensen, A. L.; Sunderland, E. M. Mercury Biogeochemical Cycling in the Ocean and Policy Implications. *Environ. Res.* **2012**, *119*, 101–117. https://doi.org/10.1016/j.envres.2012.03.013.

(5) Bowman, K. L.; Lamborg, C. H.; Agather, A. M. A Global Perspective on Mercury Cycling in the Ocean. *Sci. Total Environ.* **2020**, *710*, 136166. https://doi.org/10.1016/j.scitotenv.2019.136166.

(6) Soerensen, A. L.; Jacob, D. J.; Schartup, A. T.; Fisher, J. A.; Lehnherr, I.; Louis, V. L. S.;

Heimbürger, L.; Sonke, J. E.; Krabbenhoft, D. P.; Sunderland, E. M. A Mass Budget for Mercury and Methylmercury in the Arctic Ocean. *Global Biogeochem. Cycles* **2016**, *30* (4), 560–575. https://doi.org/10.1002/2015GB005280.

(7) Larose, C.; Dommergue, A.; Marusczak, N.; Coves, J.; Ferrari, C. P.; Schneider, D. Bioavailable Mercury Cycling in Polar Snowpacks. *Environ. Sci. Technol.* **2011**, *45*, 2150–2156. https://doi.org/10.1021/es103016x.

(8) Beattie, S. A.; Armstrong, D.; Chaulk, A.; Comte, J.; Gosselin, M.; Wang, F. Total and Methylated Mercury in Arctic Multiyear Sea Ice. *Environ. Sci. Technol.* **2014**, *48* (10), 5575–5582. https://doi.org/10.1021/es5008033.

(9) Sonke, J. E.; Teisserenc, R.; Heimbürger-Boavida, L.-E.; Petrova, M. V.; Marusczak, N.; Le Dantec, T.; Chupakov, A. V.; Li, C.; Thackray, C. P.; Sunderland, E. M.; Tananaev, N.; Pokrovsky, O. S. Eurasian River Spring Flood Observations Support Net Arctic Ocean Mercury Export to the Atmosphere and Atlantic Ocean. *Proc. Natl. Acad. Sci.* **2018**, 201811957. https://doi.org/10.1073/pnas.1811957115.

(10) Obrist, D.; Agnan, Y.; Jiskra, M.; Olson, C. L.; Dominique, P.; Hueber, J.; Moore, C. W.; Sonke, J.; Helmig, D. Tundra Uptake of Atmospheric Elemental Mercury Drives Arctic Mercury Pollution. *Nat. Publ. Gr.* **2017**, *547* (7662), 201–204. https://doi.org/10.1038/nature22997.

(11) Kirk, J.; St. Louis, V. L.; Hintelmann, H.; Lehnherr, I.; Else, B.; Poissant, L. Methylated Mercury Species in Marine Waters of the Canadian High and Sub Arctic. *Env. Sci Technol* **2008**, *42* (22), 8367–8373. https://doi.org/https://doi.org/10.1021/es801635m.

(12) Gionfriddo, C. M.; Tate, M. T.; Wick, R. R.; Schultz, M. B.; Zemla, A.; Thelen, M. P.; Schofield, R.; Krabbenhoft, D. P.; Holt, K. E.; Moreau, J. W. Microbial Mercury Methylation in Antarctic Sea Ice. *Nat. Microbiol.* **2016**, *1* (10), 16127.

https://doi.org/10.1038/nmicrobiol.2016.127.

(13) Heimbürger, L. E.; Sonke, J. E.; Cossa, D.; Point, D.; Lagane, C.; Laffont, L.; Galfond, B. T.; Nicolaus, M.; Rabe, B.; van der Loeff, M. R. Shallow Methylmercury Production in the Marginal Sea Ice Zone of the Central Arctic Ocean. *Sci. Rep.* **2015**, *5*, 10318. https://doi.org/10.1038/srep10318.

(14) Villar, E.; Cabrol, L.; Heimbürger-Boavida, L. E. Widespread Microbial Mercury Methylation Genes in the Global Ocean. *Environ. Microbiol. Rep.* **2020**, *12* (3). https://doi.org/10.1111/1758-2229.12829.

(15) AMAP. *Arctic Monitoring and Assessment Program 2011: Mercury in the Arctic*; 2011.

(16) AMAP. *AMAP Assessment 2018: Biological Effects of Contaminants on Arctic Wildlife and Fish*; 2018.

(17) Thompson, D. R.; Furness, R. W.; Walsh, P. M. Historical Changes in Mercury Concentrations in the Marine Ecosystem of the North and North-East Atlantic Ocean as Indicated by Seabird Feathers. *J. Appl. Ecol.* **1992**, *29* (1), 79–84. https://doi.org/10.2307/2404350.

(18) Carravieri, A.; Cherel, Y.; Jaeger, A.; Churlaud, C.; Bustamante, P. Penguins as Bioindicators of Mercury Contamination in the Southern Indian Ocean: Geographical and Temporal Trends. *Environ. Pollut.* **2016**, *213*, 195–205. https://doi.org/10.1016/j.envpol.2016.02.010.

(19) Rigét, F.; Braune, B.; Bignert, A.; Wilson, S.; Aars, J.; Born, E.; Dam, M.; Dietz, R.; Evans, M.; Evans, T.; Gamberg, M.; Gantner, N.; Green, N.; Gunnlaugsdóttir, H.; Kannan, K.; Letcher, R.; Muir, D.; Roach, P.; Sonne, C.; Stern, G.; Wiig, O. Temporal Trends of Hg in Arctic Biota, an Update. *Sci. Total Environ.* **2011**, *409* (18), 3520–3526. https://doi.org/10.1016/j.scitotenv.2011.05.002.

(20) Dietz, R.; Sonne, C.; Basu, N.; Braune, B.; O'Hara, T.; Letcher, R. J.; Scheuhammer, T.; Andersen, M.; Andreasen, C.; Andriashek, D.; Asmund, G.; Aubail, A.; Baagøe, H.; Born, E. W.; Chan, H. M.; Derocher, A. E.; Grandjean, P.; Knott, K.; Kirkegaard, M.; Krey, A.; Lunn, N.; Messier, F.; Obbard, M.; Olsen, M. T.; Ostertag, S.; Peacock, E.; Renzoni, A.; Rigét, F. F.; Skaare, J. U.; Stern, G.; Stirling, I.; Taylor, M.; Wiig, Ø.; Wilson, S.; Aars, J. What Are the Toxicological Effects of Mercury in Arctic Biota? *Sci. Total Environ.* **2013**, *443*, 775–790. https://doi.org/10.1016/j.scitotenv.2012.11.046.

(21) Albert, C.; Renedo, M.; Bustamante, P.; Fort, J. Using Blood and Feathers to Investigate Large-Scale Hg Contamination in Arctic Seabirds: A Review. *Environ. Res.* **2019**, *177* (July), 108588. https://doi.org/10.1016/j.envres.2019.108588.

(22) Fort, J.; Robertson, G. J.; Grémillet, D.; Traisnel, G.; Bustamante, P. Spatial Ecotoxicology: Migratory Arctic Seabirds Are Exposed to Mercury Contamination While Overwintering in the Northwest Atlantic. *Environ. Sci. Technol.* **2014**, *48* (11560–11567). https://doi.org/10.1021/es504045g.

(23) Fleishman, A. B.; Orben, R. A.; Kokubun, N.; Will, A.; Paredes, R.; Ackerman, J. T.; Takahashi, A.; Kitaysky, A. S.; Shaffer, S. A. Wintering in the Western Subarctic Pacific Increases Mercury Contamination of Red-Legged Kittiwakes. *Environ. Sci. Technol.* **2019**, *53* (22), 13398–13407. https://doi.org/10.1021/acs.est.9b03421.

(24) Renedo, M.; Amouroux, D.; Pedrero, Z.; Bustamante, P.; Cherel, Y. Identification of Sources and Bioaccumulation Pathways of MeHg in Subantarctic Penguins : A Stable Isotopic Investigation. *Sci. Rep.* **2018**, *8* (8865). https://doi.org/10.1038/s41598-018-27079-9.

(25) Point, D.; Sonke, J. E.; Day, R. D.; Roseneau, D. G.; Hobson, K. A.; Pol, S. S. Vander; Moors, A. J.; Pugh, R. S.; Donard, O. F. X.; Becker, P. R. Methylmercury Photodegradation Influenced by Sea-Ice Cover in Arctic Marine Ecosystems. *Nat. Geosci.*

2011, *4* (1), 1–7. https://doi.org/10.1038/ngeo1049.

(26) Day, R. D.; Roseneau, D. G.; Berail, S.; Hobson, K. a.; Donard, O. F. X.; Vander Pol, S. S.; Pugh, R. S.; Moors, A. J.; Long, S. E.; Becker, P. R. Mercury Stable Isotopes in Seabird Eggs Reflect a Gradient from Terrestrial Geogenic to Oceanic Mercury Reservoirs. *Environ. Sci. Technol.* **2012**, *46* (10), 5327–5335. https://doi.org/10.1021/es2047156.

(27) Blum, J. D.; Sherman, L. S.; Johnson, M. W. Mercury Isotopes in Earth and Environmental Sciences. *Annu. Rev. Earth Planet. Sci.* **2014**, *42*, 249–269. https://doi.org/10.1146/annurev-earth-050212-124107.

(28) Li, M.; Sherman, L. S.; Blum, J. D.; Grandjean, P.; Mikkelsen, B.; Weihe, P.; Sunderland, E. M.; Shine, J. P. Assessing Sources of Human Methylmercury Exposure Using Stable Mercury Isotopes. *Environ. Sci. Technol.* **2014**, *48* (15), 8800–8806. https://doi.org/10.1021/es500340r.

(29) Cransveld, A. A. E.; Amouroux, D.; Tessier, E.; Koutrakis, E.; Ozturk, A. A.; Bettoso, N.; Mieiro, C. L.; Berail, S.; Barre, J. P. G.; Sturaro, N.; Schnitzler, J. G.; Das, K. Mercury Stable Isotopes Discriminate Different Populations of European Seabass and Trace Potential Hg Sources around Europe. *Environ. Sci. Technol.* **2017**, *51* (21), 12219–12228. https://doi.org/10.1021/acs.est.7b01307.

(30) Kritee, K.; Barkay, T.; Blum, J. D. Mass Dependent Stable Isotope Fractionation of Mercury during Mer Mediated Microbial Degradation of Monomethylmercury. *Geochim. Cosmochim. Acta* **2009**, *73* (5), 1285–1296. https://doi.org/10.1016/j.gca.2008.11.038.

(31) Kritee, K.; Blum, J. D.; Barkay, T. Mercury Stable Isotope Fractionation during Reduction of Hg(II) by Different Microbial Pathways. *Environ. Sci. Technol.* **2008**, *42* (24), 9171–9177. https://doi.org/10.1021/es801591k.

(32) Zheng, W.; Foucher, D.; Hintelmann, H. Mercury Isotope Fractionation during

Volatilization of Hg(0) from Solution into the Gas Phase. *J. Anal. At. Spectrom.* **2007**, *22* (9), 1097. https://doi.org/10.1039/b705677j.

(33) Kwon, S. Y.; Blum, J. D.; Chirby, M. a; Chesney, E. J. Application of Mercury Isotopes for Tracing Trophic Transfer and Internal Distribution of Mercury in Marine Fish Feeding Experiments. *Environ. Toxicol. Chem.* **2013**, *32* (10), 2322–2330. https://doi.org/10.1002/etc.2313.

(34) Kwon, S. Y.; Blum, J. D.; Carvan, M. J.; Basu, N.; Head, J. A.; Madenjian, C. P.; David, S. R. Absence of Fractionation of Mercury Isotopes during Trophic Transfer of Methylmercury to Freshwater Fish in Captivity. *Environ. Sci. Technol.* **2012**, *46* (14), 7527–7534. https://doi.org/10.1021/es300794q.

(35) Masbou, J.; Point, D.; Sonke, J. E.; Frappart, F.; Perrot, V.; Amouroux, D.; Richard, P.; Becker, P. R. Hg Stable Isotope Time Trend in Ringed Seals Registers Decreasing Sea Ice Cover in the Alaskan Arctic. *Env. Sci Technol* **2015**, *49*, 8977–8985. https://doi.org/10.1021/es5048446.

(36) Chen, J.; Hintelmann, H.; Feng, X.; Dimock, B. Unusual Fractionation of Both Odd and Even Mercury Isotopes in Precipitation from Peterborough, ON, Canada. *Geochim. Cosmochim. Acta* **2012**, *90*, 33–46. https://doi.org/10.1016/j.gca.2012.05.005.

(37) Gratz, L. E.; Keeler, G. J.; Blum, J. D.; Sherman, L. S. Isotopic Composition and Fractionation of Mercury in Great Lakes Precipitation and Ambient Air. *Environ. Sci. Technol.* **2010**, *44* (20), 7764–7770. https://doi.org/10.1021/es100383w.

(38) Sherman, L. S.; Blum, J. D.; Douglas, T. A.; Steffen, A. Frost Flowers Growing in the Arctic Ocean-Atmosphere-Sea Ice-Snow Interface: 2. Mercury Exchange between the Atmosphere, Snow, and Frost Flowers. *J. Geophys. Res. Atmos.* **2012**, *117* (3), 1–10. https://doi.org/10.1029/2011JD016186.

(39) Demers, J. D.; Blum, J. D.; Zak, D. R. Mercury Isotopes in a Forested Ecosystem: Implications for Air-Surface Exchange Dynamics and the Global Mercury Cycle. *Global Biogeochem. Cycles* **2013**, *27* (1), 222–238. https://doi.org/10.1002/gbc.20021.

(40) Enrico, M.; Roux, G. Le; Marusczak, N.; Heimbürger, L. E.; Claustres, A.; Fu, X.; Sun, R.; Sonke, J. E. Atmospheric Mercury Transfer to Peat Bogs Dominated by Gaseous Elemental Mercury Dry Deposition. *Environ. Sci. Technol.* **2016**, *50* (5), 2405–2412. https://doi.org/10.1021/acs.est.5b06058.

(41) Keslinka, L. K.; Wojczulanis-Jakubas, K.; Jakubas, D.; Neubauer, G. Determinants of the Little Auk (Alle Alle) Breeding Colony Location and Size in W and NW Coast of Spitsbergen. *PLoS One* **2019**, *14* (3). https://doi.org/10.1371/journal.pone.0212668.

(42) Kovacs, K.; Lydersen, C. *Birds and Mammals of Svalbard. Tromsø: Norwegian Polar Institute*; 2006.

(43) Harding, A. M. A.; Hobson, K. A.; Walkusz, W.; Dmoch, K.; Karnovsky, N. J.; Van Pelt, T. I.; Lifjeld, J. T. Can Stable Isotope (Δ13C and Δ15N) Measurements of Little Auk (Alle Alle) Adults and Chicks Be Used to Track Changes in High-Arctic Marine Foodwebs? *Polar Biol.* **2008**, *31* (6), 725–733. https://doi.org/10.1007/s00300-008-0413-4.

(44) Grémillet, D.; Welcker, J.; Karnovsky, N. J.; Walkusz, W.; Hall, M. E.; Fort, J.; Brown, Z. W.; Speakman, J. R.; Harding, A. M. A. Little Auks Buffer the Impact of Current Arctic Climate Change. *Mar. Ecol. Prog. Ser.* **2012**, *454*, 197–206. https://doi.org/10.3354/meps09590.

(45) Fort, J.; Moe, B.; Strøm, H.; Grémillet, D.; Welcker, J.; Schultner, J.; Jerstad, K.; Johansen, K. L.; Phillips, R. A.; Mosbech, A. Multicolony Tracking Reveals Potential Threats to Little Auks Wintering in the North Atlantic from Marine Pollution and Shrinking Sea Ice Cover. *Divers. Distrib.* **2013**, *19* (10), 1322–1332.

https://doi.org/10.1111/ddi.12105.

(46) Fort, J.; Gremillet, D.; Traisnel, G.; Amelineau, F.; Bustamante, P. Does Temporal Variation of Mercury Levels in Arctic Seabirds Reflect Changes in Global Environmental Contamination, or a Modification of Arctic Marine Food Web Functioning ? *Environ. Pollut.* **2016**, *211*, 382–388. https://doi.org/10.1016/j.envpol.2015.12.061.

(47) Furness, R. W.; Muirhead, S. J.; Woodburn, M. Using Bird Feathers to Measure Mercury in the Environment: Relationships between Mercury Content and Moult. *Mar. Pollut. Bull.* **1986**, *17* (1), 27–30. https://doi.org/10.1016/0025-326X(86)90801-5.

(48) Honda, K.; Nasu, T.; Tatsukawa, R. Seasonal Changes in Mercury Accumulation in the Black-Eared Kite, *Milvus Migrans Lineatus*. *Environ. Pollut. Ser. A, Ecol. Biol.* **1986**, *42*, 325–334. https://doi.org/10.1016/0143-1471(86)90016-4.

(49) Hobson, K. A.; Clark, R. G. Assessing Avian Diets Using Stable Isotopes I: Turnover of 13C in Tissues. *Condor* **1992**, *94* (1), 181–188. https://doi.org/https://doi.org/10.2307/1368807.

(50) Bearhop, S.; Waldron, S.; Votier, S. C.; Furness, R. W. Factors That Influence Assimilation Rates and Fractionation of Nitrogen and Carbon Stable Isotopes in Avian Blood and Feathers. *Physiol. Biochem. Zool.* **2002**, *75* (5). https://doi.org/https://doi.org/10.1086/342800.

(51) Fort, J.; Beaugrand, G.; Grémillet, D.; Phillips, R. A. Biologging, Remotely-Sensed Oceanography and the Continuous Plankton Recorder Reveal the Environmental Determinants of a Seabird Wintering Hotspot. *PLoS One* **2012**, *7* (7). https://doi.org/10.1371/journal.pone.0041194.

(52) Grissot, A.; Graham, I. M.; Quinn, L.; Bråthen, V. S.; Thompson, P. M. Breeding Status Influences Timing but Not Duration of Moult in the Northern Fulmar Fulmarus Glacialis.

Ibis (Lond. 1859). **2019**, 1–14. https://doi.org/10.1111/ibi.12714.

(53) Carravieri, A.; Bustamante, P.; Churlaud, C.; Fromant, A.; Cherel, Y. Moulting Patterns Drive Within-Individual Variations of Stable Isotopes and Mercury in Seabird Body Feathers: Implications for Monitoring of the Marine Environment. *Mar. Biol.* **2014**, *161*, 963–968. https://doi.org/10.1007/s00227-014-2394-x.

(54) Peterson, S. H.; Ackerman, J. T.; Toney, M.; Herzog, M. P. Mercury Concentrations Vary Within and Among Individual Bird Feathers: A Critical Evaluation and Guidelines for Feather Use in Mercury Monitoring Programs. *Environ. Toxicol. Chem.* **2019**, *38* (6), 1164–1187. https://doi.org/10.1002/etc.4430.

(55) Renedo, M.; Bustamante, P.; Tessier, E.; Pedrero, Z.; Cherel, Y.; Amouroux, D. Assessment of Mercury Speciation in Feathers Using Species-Specific Isotope Dilution Analysis. *Talanta* **2017**, *174*, 100–110. https://doi.org/10.1016/j.talanta.2017.05.081.

(56) Renedo, M.; Amouroux, D.; Duval, B.; Carravieri, A.; Tessier, E.; Barre, J.; Bérail, S.; Pedrero, Z.; Cherel, Y.; Bustamante, P. Seabird Tissues As Efficient Biomonitoring Tools for Hg Isotopic Investigations: Implications of Using Blood and Feathers from Chicks and Adults. *Environ. Sci. Technol.* **2018**, *52* (7), 4227–4234. https://doi.org/10.1021/acs.est.8b00422.

(57) Yamakawa, A.; Takeuchi, A.; Shibata, Y.; Berail, S.; Donard, O. F. X. Determination of Hg Isotopic Compositions in Certified Reference Material NIES No. 13 Human Hair by Cold Vapor Generation Multi-Collector Inductively Coupled Plasma Mass Spectrometry. *Accredit. Qual. Assur.* **2016**, *21* (13), 197–202. https://doi.org/10.1007/s00769-016-1196-x.

(58) R Core Team, 2016: A Language and Environment for Statistical Computing. R Foundation for Statistical Computing, Vienna, Austria.

(59) Bates, D.; Mächler, M.; Bolker, B. M.; Walker, S. C. Fitting Linear Mixed-Effects Models Using Lme4. *J. Stat. Softw.* **2015**, *67* (1). https://doi.org/10.18637/jss.v067.i01.

(60) Salmerón, R.; García, C. B.; García, J. Variance Inflation Factor and Condition Number in Multiple Linear Regression. *J. Stat. Comput. Simul.* **2018**, *88* (12), 2365–2384. https://doi.org/https://doi.org/10.1080/00949655.2018.1463376.

(61) Zuur, A. F.; Ieno, E. N.; Walker, N. J.; Saveliev, A. A.; Smith, G. M. Mixed Effects Models and Extensions in Ecology with R. *J. Stat. Softw.* **2009**, *32* (Book Review 1), 1–4. https://doi.org/10.18637/jss.v032.b01.

(62) Meredith, M. M. Package ' Wiqid .' **2020**.

(63) Jaeger, B. C. Computes R Squared for Mixed (Multilevel) Model. *Packag. 'r2glmm'* **2017**, 12.

(64) Davis, W. C.; Vander Pol, S. S.; Schantz, M. M.; Long, S. E.; Day, R. D.; Christopher, S. J. An Accurate and Sensitive Method for the Determination of Methylmercury in Biological Specimens Using GC-ICP-MS with Solid Phase Microextraction. *J. Anal. At. Spectrom.* **2004**, *19* (12), 1546–1551. https://doi.org/10.1039/b412668h.

(65) Bond, A. L.; Diamond, A. W. Total and Methyl Mercury Concentrations in Seabird Feathers and Eggs. *Arch. Environ. Contam. Toxicol* **2009**, 286–291. https://doi.org/10.1007/s00244-008-9185-7.

(66) Rosing-Asvid, A.; Hedeholm, R.; Arendt, K. E.; Fort, J.; Robertson, G. J. Winter Diet of the Little Auk (Alle Alle) in the Northwest Atlantic. *Polar Biol.* **2013**, *36* (11), 1601–1608. https://doi.org/10.1007/s00300-013-1379-4.

(67) Fort, J.; Cherel, Y.; Harding, A. M. A.; Welcker, J.; Jakubas, D.; Steen, H.; Karnovsky, N. J.; Grémillet, D. Geographic and Seasonal Variability in the Isotopic Niche of Little Auks. *Mar. Ecol. Prog. Ser.* **2010**, *414*, 293–302. https://doi.org/10.3354/meps08721.

(68) Welcker, J.; Harding, A. M. A.; Karnovsky, N. J.; Steen, H.; Strøm, H.; Gabrielsen, G. W. Flexibility in the Bimodal Foraging Strategy of a High Arctic Alcid, the Little Auk Alle Alle. *J. Avian Biol.* **2009**, *40* (4), 388–399. https://doi.org/10.1111/j.1600-048X.2008.04620.x.

(69) Hobson, K. A.; Clark, R. G. Assessing Avian Diets Using Stable Isotopes II : Factors Influencing Diet-Tissue Fractionation. *Condor* **1992**, *94* (1), 189–197. https://doi.org/https://doi.org/10.2307/1368808.

(70) Graham, B. S.; Koch, P. L.; Newsome, S. D.; McMahon, K. W.; Aurioles, D. Using Isoscapes to Trace the Movements and Foraging Behavior of Top Predators in Oceanic Ecosystems. In *Isoscapes: Understanding Movement, Pattern, and Process on Earth Through Isotope Mapping*; 2010; pp 299–318. https://doi.org/https://doi.org/10.1007/978-90-481-3354-3_14.

(71) McMahon, K. W.; Hamady, L. L.; Thorrold, S. R. A Review of Ecogeochemistry Approaches to Estimating Movements of Marine Animals. *Limnol. Oceanogr.* **2013**, *58* (2), 697–714. https://doi.org/10.4319/lo.2013.58.2.0697.

(72) Kürten, B.; Painting, S. J.; Struck, U.; Polunin, N. V. C.; Middelburg, J. J. Tracking Seasonal Changes in North Sea Zooplankton Trophic Dynamics Using Stable Isotopes. *Biogeochemistry* **2013**, *113* (1–3), 167–187. https://doi.org/10.1007/s10533-011-9630-y.

(73) Renedo, M.; Pedrero, Z.; Amouroux, D.; Cherel, Y.; Bustamante, P. Mercury Isotopes of Key Tissues Document Mercury Metabolic Processes in Seabirds. *Chemosphere* **2020**, *12777*. https://doi.org/10.1016/j.chemosphere.2020.127777.

(74) Stempniewicz, L.; Skakuj, M.; Iliszko, L. The Little Auk Alle Alle Polaris of Franz Josef Land: A Comparison with Svalbard Alle a. Alle Populations. *Polar Res.* **1996**, *15* (1), 1–10. https://doi.org/10.3402/polar.v15i1.6632.

(75) Motta, L. C.; Blum, J. D.; Johnson, M. W.; Umhau, B. P.; Popp, B. N.; Washburn, S. J.; Drazen, J. C.; Benitez-Nelson, C. R.; Hannides, C. C. S.; Close, H. G.; Lamborg, C. H. Mercury Cycling in the North Pacific Subtropical Gyre as Revealed by Mercury Stable Isotope Ratios. *Global Biogeochem. Cycles* **2019**, *33* (6), 777–794. https://doi.org/10.1029/2018GB006057.

(76) Burt, A.; Wang, F.; Pučko, M.; Mundy, C. J.; Gosselin, M.; Philippe, B.; Poulin, M.; Tremblay, J. É.; Stern, G. A. Mercury Uptake within an Ice Algal Community during the Spring Bloom in First-Year Arctic Sea Ice. *J. Geophys. Res. Ocean.* **2013**, *118* (9), 4746–4754. https://doi.org/10.1002/jgrc.20380.

(77) Schartup, A. T.; Balcom, P. H.; Soerensen, A. L.; Gosnell, K. J.; Calder, R. S. D.; Mason, R. P.; Sunderland, E. M. Freshwater Discharges Drive High Levels of Methylmercury in Arctic Marine Biota. *Proc. Natl. Acad. Sci.* **2015**, *112* (38), 11789–11794. https://doi.org/10.1073/pnas.1505541112.

(78) Renedo, M.; Bustamante, P.; Cherel, Y.; Pedrero, Z.; Tessier, E.; Amouroux, D. A "Seabird-Eye" on Mercury Stable Isotopes and Cycling in the Southern Ocean. *Sci. Total Environ.* **2020**, *742*, 140499. https://doi.org/10.1016/j.scitotenv.2020.140499.

(79) Masbou, J.; Sonke, J. E.; Amouroux, D.; Guillou, G.; Becker, P. R.; Point, D. Hg-Stable Isotope Variations in Marine Top Predators of the Western Arctic Ocean. *ACS Earth Sp. Chem.* **2018**, *2* (0), 479–490. https://doi.org/10.1021/acsearthspacechem.8b00017.

(80) Lynch-Stieglitz, J.; Stocker, T. F.; Broecker, W. S.; Fairbanks, R. G. The Influence of Air-sea Exchange on the Isotopic Composition of Oceanic Carbon: Observations and Modeling. *Global Biogeochem. Cycles* **1995**, *9* (4), 653–665. https://doi.org/https://doi.org/10.1029/95GB02574.

(81) Gruber, N.; Keeling, D.; Bacastow, R. B.; Guenther, P. R.; Lueker, T. J.; Wahlen, M.;

Meijer, H. a J.; Mook, W. G.; Stocker, T. F. Spatiotemporal Patterns of Carbon-13 in the Global Surface Oceans and the Oceanic Suess Effect. *Global Biogeochem. Cycles* **1999**, *13* (2), 307–335. https://doi.org/10.1029/1999GB900019.

(82) Fontela, M.; García-Ibáñez, M. I.; Hansell, D. A.; Mercier, H.; Pérez, F. F. Dissolved Organic Carbon in the North Atlantic Meridional Overturning Circulation. *Sci. Rep.* **2016**, *6*, 1–9. https://doi.org/10.1038/srep26931.

(83) Li, M.; Schartup, A. T.; Valberg, A. P.; Ewald, J. D.; David, P.; Yin, R.; Balcom, P. H.; Sunderland, E. M. Environmental Origins of Methylmercury Accumulated in Subarctic Estuarine Fish Indicated by Mercury Stable Isotopes. *Env. Sci Technol* **2016**, *50*, 11559–15568. https://doi.org/10.1021/acs.est.6b03206.

Supporting Information

Contrasting spatial and seasonal trends of methylmercury exposure pathways of Arctic seabirds: combination of large-scale tracking and stable isotopic approaches

Marina Renedo[1,2,*], David Amouroux[2], Céline Albert[1], Sylvain Bérail[2], Vegard S. Bråthen[3], Maria Gavrilo[4], David Grémillet[5,6], Hálfdán H. Helgason[7], Dariusz Jakubas[8], Anders Mosbech[9], Hallvard Strøm[7], Emmanuel Tessier[2] , Katarzyna Wojczulanis-Jakubas[8], Paco Bustamante[1,10], Jérôme Fort[1*]

[1] Littoral Environnement et Sociétés (LIENSs), UMR 7266 CNRS- La Rochelle Université, 2 rue Olympe de Gouges, 17000 La Rochelle, France

[2] Universite de Pau et des Pays de l'Adour, E2S UPPA, CNRS, IPREM, Institut des Sciences Analytiques et de Physico-chimie pour l'Environnement et les matériaux, Pau, France

[3] Norwegian Institute for Nature Research, Trondheim, Norway

[4] Arctic and Antarctic Research Institute, 38 Bering Street, 199397, Saint-Petersburg, Russia

[5] Centre d'Etudes Biologiques de Chizé, UMR 7372 CNRS –La Rochelle Université, 405 Route de Prissé la Charrière 79360 Villiers-en-Bois, France

[6] Percy FitzPatrick Institute, DST/NRF Centre of Excellence, University of Cape Town, Rondebosch, South Africa

[7] Norwegian Polar Institute, Tromsø, Norway

[8] Gdańsk University, Faculty of Biology, Gdańsk, Poland

[9] Aarhus University, Department of Bioscience, Roskilde, Denmark

[10] Institut Universitaire de France (IUF), 1 rue Descartes, 75005 Paris, France

**Corresponding authors:* marina.renedo@ird.fr, jerome.fort@univ-lr.fr

Table of contents

Experimental: Hg isotopic composition analyses

Hg isotopic compositions of samples are reported using delta notation according to the following equations:

$$\delta^{xxx}\,Hg = [(^{xxx/198}Hg_{sample} / {}^{xxx/198}Hg_{\,NIST\,3133}) - 1)] \cdot 1000\ (‰) \qquad (1)$$

MIF signatures are expressed using capital delta notation, as suggested elsewhere [1], according to the following equations:

$$\Delta^{204}\,Hg = \delta^{204}\,Hg - (1.493 \cdot \delta^{202}\,Hg) \qquad (2)$$

$$\Delta^{201}\,Hg = \delta^{201}\,Hg - (0.752 \cdot \delta^{202}\,Hg) \qquad (3)$$

$$\Delta^{200}\,Hg = \delta^{200}\,Hg - (0.502 \cdot \delta^{202}\,Hg) \qquad (4)$$

$$\Delta^{199}\,Hg = \delta^{199}\,Hg - (0.252 \cdot \delta^{202}\,Hg) \qquad (5)$$

Supplementary figures

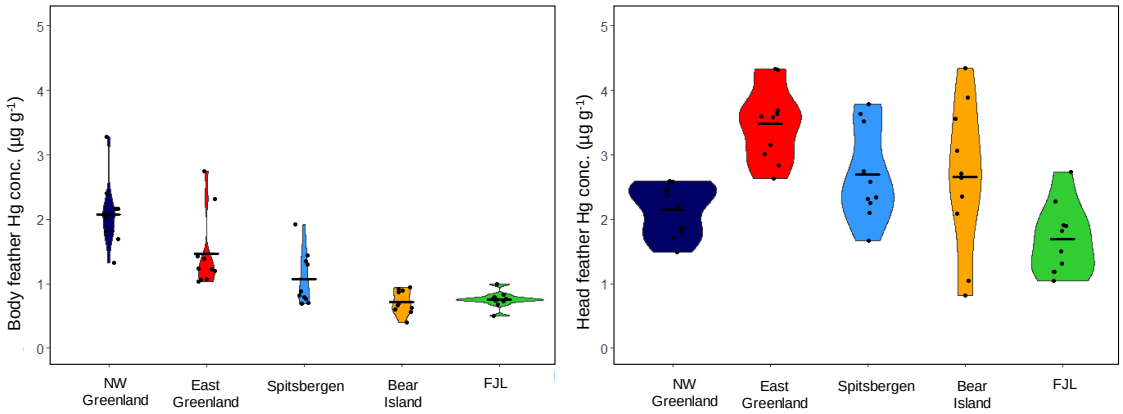

Figure S1. Violin plots of total Hg concentrations (µg·g^{-1}, dw) of body and head feathers of little auks (both n=50). Black lines indicate mean values.

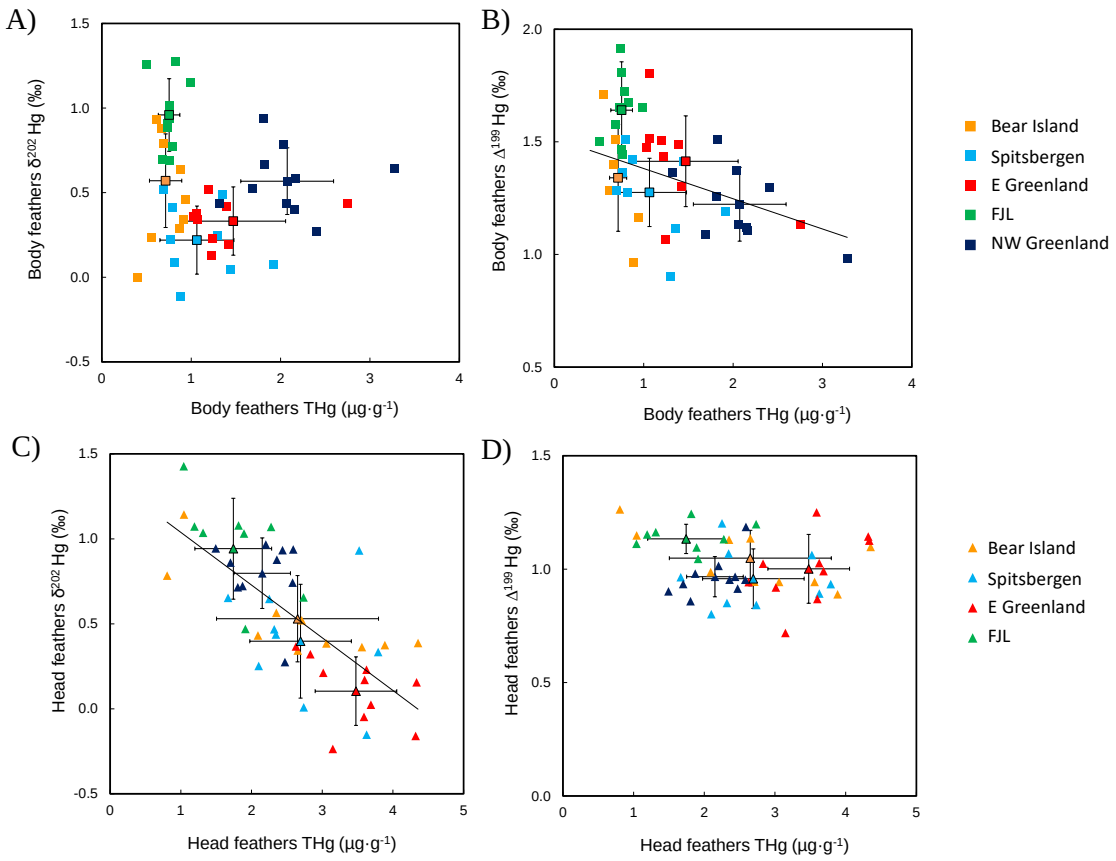

Figure S2. Hg concentration (µg·g^{-1}) as a function of δ^{202}Hg and Δ^{199}Hg (A) of little auk body feathers (summer) and head feathers (winter). Regression equations are A) Slope: -0.112±0.077, intercept: 0.678±0.107, R^2=0.05, p=0.156; B) Slope: -0.202±0.048, intercept: 1.631±0.066, R^2=0.29, p=0.0003; C) Slope: -0.310±0.044, intercept: 1.348±0.122, R^2=0.52, p<0.0001; D) Slope: -0.026±0.021, intercept: 1.085±0.057, R^2=0.03, p=0.225.

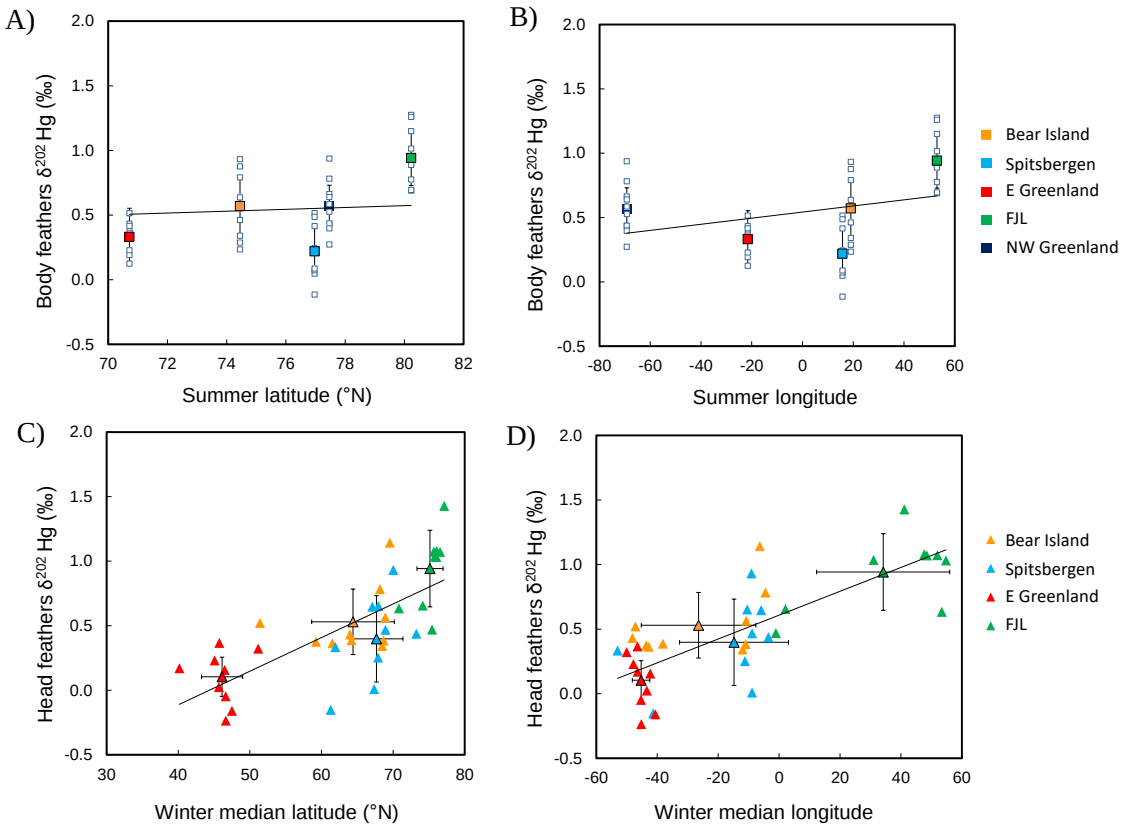

Figure S3. Hg MDF (δ^{202}Hg) of little auk body feathers (summer) as a function of (A) latitude and (B) longitude of their breeding sites and head feathers (winter) as a function of the (C) median latitude and (D) median longitude of their winter grounds. Regression equations are A) Slope: 0.053±0.015, intercept: -3.426±1.185, R^2=0.25, p<0.0001; B) Slope: 0.002±0.001, intercept: 0.543±0.047, R^2=0.08 p=0.03; C) Slope: 0.026±0.004, intercept: -0.958±0.269, R^2=0.50, p<0.0001; D) Slope: 0.001±0.001, intercept: 0.647±0.046, R^2=0.62, p<0.0001.

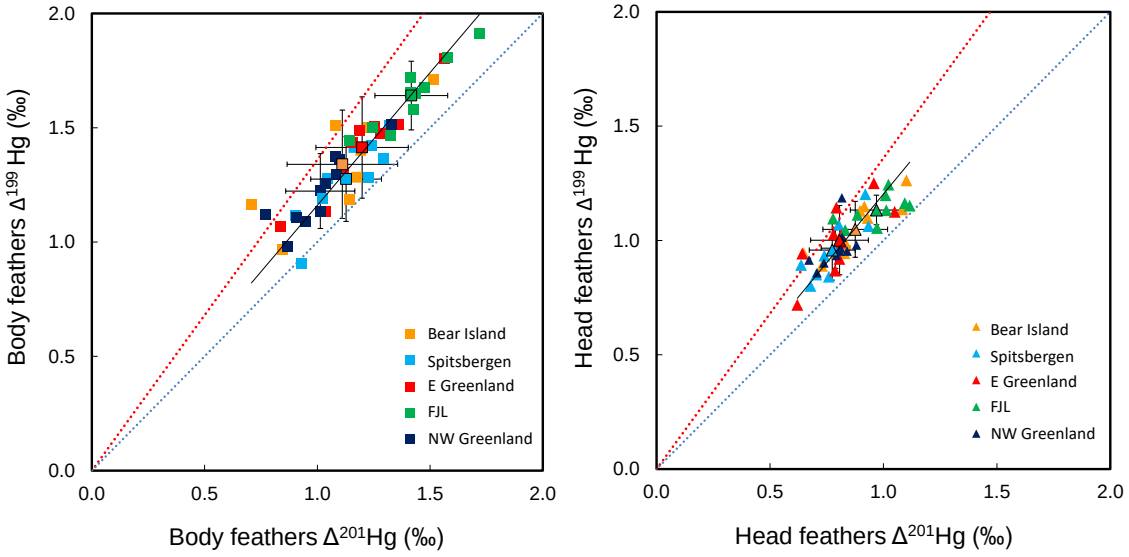

Figure S4. Δ^{199}Hg *versus* Δ^{201}Hg relationship observed in all little auks from the five populations. Overall slopes are 1.20 ± 0.08 (R^2=0.65, p<0.0001) and 1.16 ± 0.06 (R^2=0.85, p<0.0001) for head feathers and body feathers, respectively. The red dashed line represents the theoretical Δ^{199}Hg/Δ^{201}Hg slope for MeHg photodemethylation in the water column and the blue dashed line represents the theoretical Δ^{199}Hg/Δ^{201}Hg slope expected for photoreduction of inorganic Hg in the water column [1].

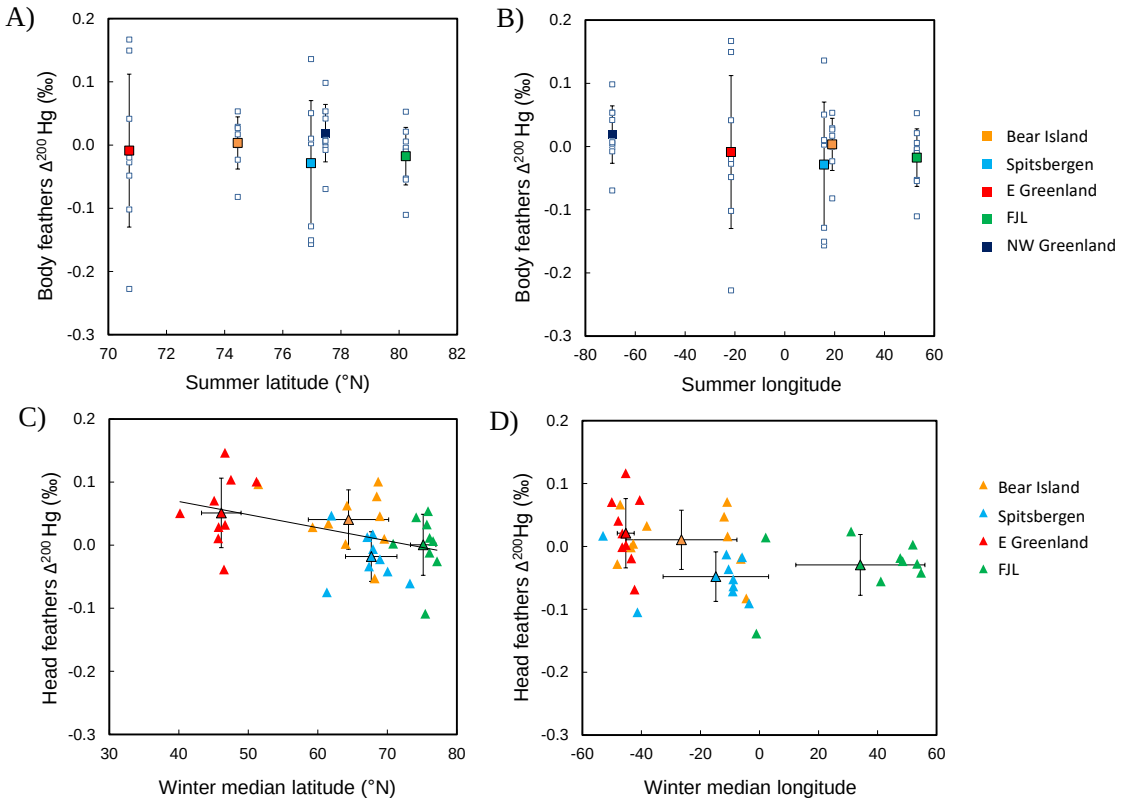

Figure S5. Hg even MIF (Δ^{200}Hg) of little auk body feathers (summer) as a function of (A) latitude and (B) longitude of their breeding sites and head feathers (winter) as a function of the (C) median latitude and (D) median longitude of their winter grounds. Regression equation are A) Slope: -0.0006±0.0035, intercept: 0.040±0.267, R^2= 0.001, p = 0.860; B) Slope: -0.0002±0.0002, intercept: -0.007±0.011, R^2 = 0.025, p = 0.291 C) Slope: -0.0002±0.0007, intercept: 0.123±0.048, R^2 = 0.19, p = 0.009; D) Slope: -0.0005±0.0002, intercept: -0.0157±0.0009, R^2 = 0.11, p = 0.050. Regression lines presented only for significant relationship between the two variables.

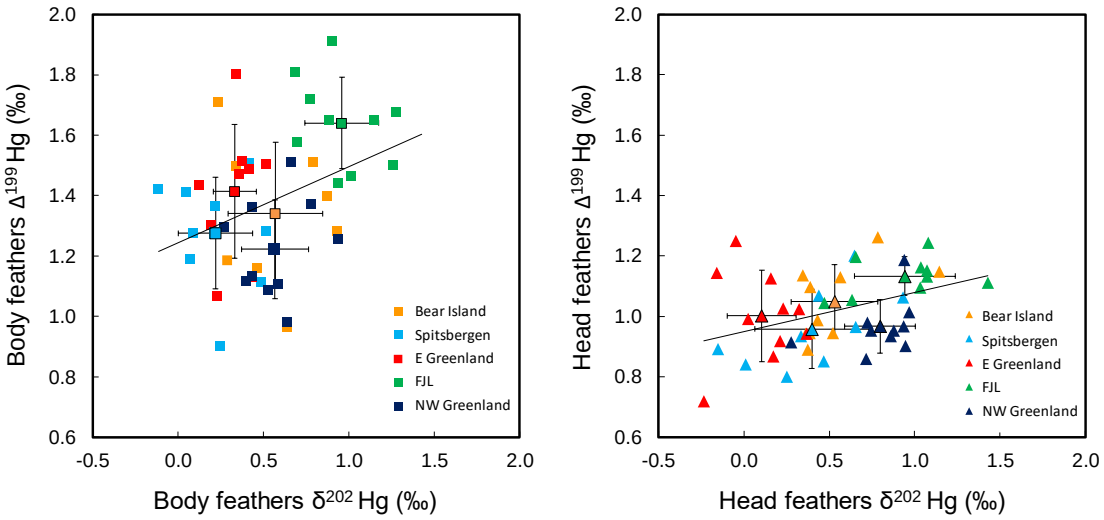

Figure S6. Hg MIF *versus* MDF values (Δ^{199}Hg *versus* δ^{202}Hg) of little auk head feathers (left figure) and body feathers (right figure). Linear regression slopes: A) Slope: 0.13±0.04, intercept: 0.95±0.03, R^2 = 0.16, p = 0.005; B) Slope: 0.23±0.10, intercept: 1.25±0.06, R^2 = 0.10, p = 0.028.

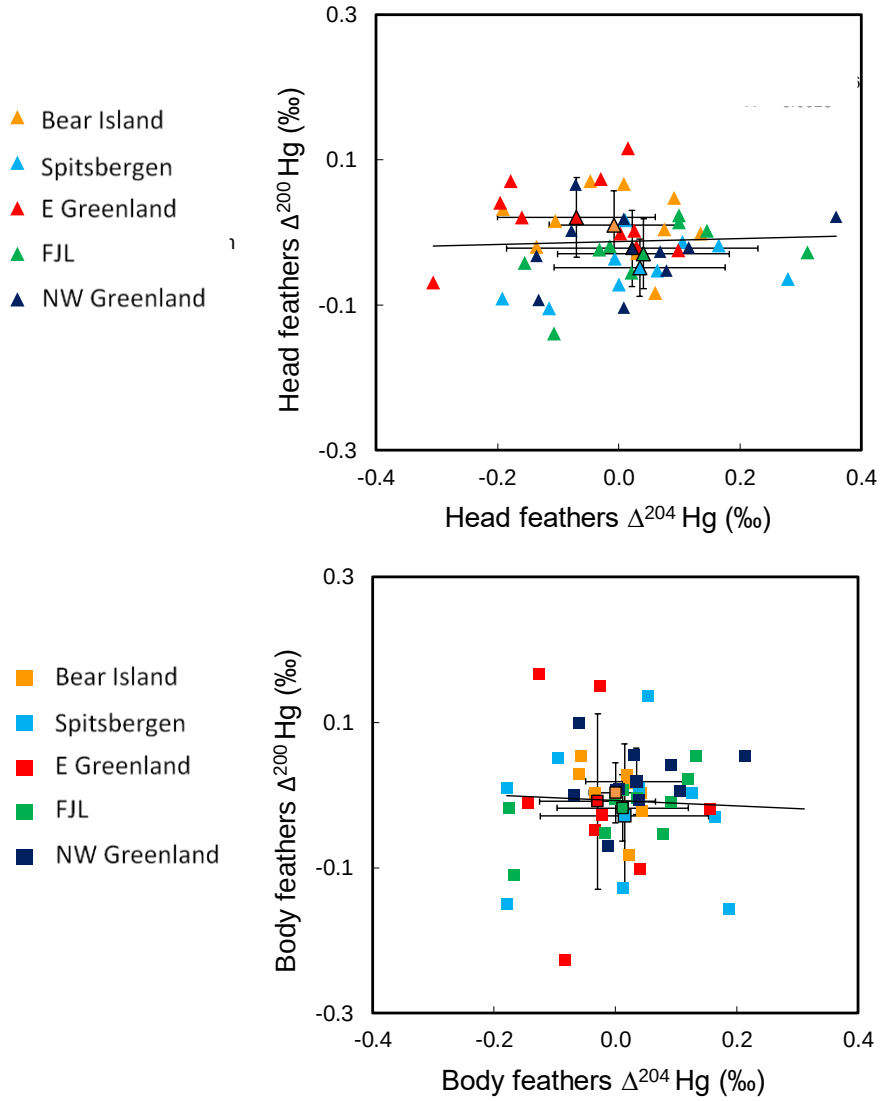

Figure S7. Hg even-MIF signatures (Δ^{200}Hg *versus* Δ^{204}Hg) of little auk head feathers (upper figure) and body feathers (lower figure) for the five populations of little auks.

Supplementary tables

Table S1. Mean values of total Hg and MeHg concentrations and percentage recoveries obtained for reference materials with validated reference concentration values: NIES-13 (human hair) and Dolt-5 (dogfish liver); and previously published intercomparison values for internal reference materials: F-KP (penguin feathers) and RBC-KP (penguin red blood cells). Values are Mean±SD. N corresponds to the number of analyses (triplicate analyses for each extract, n=3 extractions).

Reference material		n	MeHg ($\mu g\ g^{-1}$)	MeHg recovery (%)	THg ($\mu g\ g^{-1}$)	THg recovery (%)
Human hair NIES-13	This study	*9*	3.61±0.20	95±5	4.18±0.24	95±4
	Certified values		3.80±0.40		4.42±0.20	
Dogfish liver Dolt-5	This study	*9*	0.110±0.023	92±11	0.45±0.02	102±8
	Certified values		0.119±0.058		0.44±0.18	
Feathers F-KP	This study	*9*	2.51±0.11	97±5	3.88±0.90	97±2
	Average previous values [2]		2.54±0.4		3.89±0.6	
Blood RBC-KP	This study	*9*	1.93±0.41	102±1	1.76±0.46	108±3
	Average previous values [3]		1.96±0.38		1.98±0.76	

Table S2. Mean values of Hg isotopic composition obtained for reference materials with validated reference isotopic values: NIST RM 8610 (former UM-Almadén) and NIES-13 (human hair); previously published intercomparison values for internal reference materials: F-KP (penguin feathers) and RBC-KP (penguin red blood cells). Values are Mean±2SD. N means number of analyses.

Reference Material	$\delta^{204}Hg$	$\delta^{202}Hg$	$\delta^{201}Hg$	$\delta^{200}Hg$	$\delta^{199}Hg$	$\Delta^{204}Hg$	$\Delta^{201}Hg$	$\Delta^{200}Hg$	$\Delta^{199}Hg$	*n*
NIST RM 8610 (UM Almadén)										
This study										
Average (‰)	-0.80	-0.52	-0.43	-0.25	-0.16	-0.03	-0.04	0.01	-0.03	*20*
2SD (‰)	0.23	0.13	0.12	0.13	0.16	0.16	0.11	0.10	0.15	
Reference values										
Average (‰)	-0.82	-0.56	-0.46	-0.27	-0.17	-	-0.04	0.00	-0.03	
2SD (‰)	0.07	0.03	0.02	0.01	0.01	-	0.01	0.01	0.02	
NIES-13										
This study										
Average (‰)	2.87	2.08	3.01	1.13	2.30	-0.08	1.42	0.04	1.75	*3*
2SD (‰)	0.17	0.09	0.14	0.10	0.10	0.15	0.05	0.02	0.05	
Yamakawa et al. 2016[4]										
Average (‰)	2.76	1.89	2.77	0.98	2.13	-0.04	1.36	0.04	1.65	*11*
2SD (‰)	0.16	0.1	0.1	0.08	0.07	0.11	0.07	0.04	0.06	
King penguin feathers (F-KP)										
This study										
Average (‰)	2.17	1.40	2.54	0.71	2.03	0.07	1.48	0.00	1.68	*7*
2SD (‰)	0.19	0.15	0.27	0.19	0.23	0.33	0.19	0.13	0.19	
Renedo et al. 2018[3]										
Average (‰)	2.40	1.58	2.67	0.80	2.11	0.04	1.48	0.01	1.71	*17*
2SD (‰)	0.25	0.22	0.21	0.16	0.18	0.24	0.13	0.09	0.15	
King penguin blood (RBC-KP)										
This study										
Average (‰)	2.00	1.32	2.28	0.64	1.79	0.04	1.29	-0.02	1.46	*5*
2SD (‰)	0.18	0.12	0.14	0.14	0.18	0.10	0.09	0.09	0.16	
Renedo et al., 2018[3]										
Average (‰)	1.98	1.30	2.26	0.64	1.78	0.04	1.28	-0.01	1.46	*7*
2SD (‰)	0.18	0.13	0.14	0.13	0.17	0.1	0.09	0.09	0.14	

Table S3. Total Hg (THg) and MeHg concentrations (µg g^{-1}, dw) and MeHg proportion (%) in body feathers and blood of little auks. Values are Mean±SD.

Site	Latitude	Longitude	n	Tissue	MeHg (µg g^{-1})	THg (µg g^{-1})	MeHg (%)
FJL	77º47'N	-69º22W	5	body feathers	1.94±1.20	2.06±1.24	94±1
NW Greenland	70º71'N	-21º55'W	5	body feathers	2.74±0.54	2.89±0.57	95±1
Spitsbergen	76º97'N	15º78'E	5	body feathers	4.28±0.80	4.57±0.91	94±1
East Greenland	74º45'N	19º04'E	5	body feathers	4.17±1.68	4.53±2.02	93±3
FJL	77º47'N	-69º22W	5	Blood	0.36±0.13	0.40±0.14	90±4
Bear Island	80º23'N	53º01'E	5	Blood	0.45±0.24	0.50±0.27	91±1

Table S4. Total Hg concentrations (Mean ± SD, µg g^{-1}, dw) and Hg stable isotopes (Mean ± 2SD, ‰) of head and body feathers from little auks of the five studied populations. n1, number of individuals for total Hg concentration and C and N isotopic analyses; n2, number of individuals for Hg isotopic analyses). Values not sharing the same superscript letter within each group are statistically different.

Population	Feather type	n1	THg (µg g^{-1})	n2	δ^{202}Hg (‰)	Δ^{199}Hg (‰)	Δ^{200}Hg (‰)	Δ^{199}Hg/Δ^{201}Hg ratio
FJL	head feathers	10	1.74±0.54 ^{A}	9	0.94±0.30 ^{D}	1.13±0.06 ^{B}	-0.03±0.05 ^{A,B}	1.18±0.12 ^{A}
Bear Island	head feathers	10	2.65±1.15 ^{A,B}	10	0.53±0.25 ^{B,C}	1.05±0.12 ^{A,B}	0.01±0.05 ^{A,B}	1.21±0.11 ^{A}
E Greenland	head feathers	10	3.48±0.58 ^{B}	10	0.10±0.20 ^{A}	1.00±0.15 ^{A,B}	0.02±0.06 ^{B}	1.25±0.14 ^{A}
Spitsbergen	head feathers	10	2.69±0.72 ^{A,B}	9	0.40±0.33 ^{A,B}	0.96±0.13 ^{A}	-0.05±0.04 ^{A}	1.24±0.09 ^{A}
NW Greenland	head feathers	10	2.15±0.40 ^{A}	10	0.80±0.21 ^{C,D}	0.97±0.09 ^{A}	-0.02±0.01 ^{A,B}	1.23±0.10 ^{A}
FJL	body feathers	10	0.75±0.12 ^{A}	10	0.96±0.21 ^{D}	1.64±0.15 ^{B}	-0.02±0.05 ^{A}	1.16±0.05 ^{A}
Bear Island	body feathers	10	0.71±0.18 ^{A}	8	0.57±0.28 ^{B,C}	1.34±0.24 ^{A}	0.00±0.04 ^{A}	1.23±0.20 ^{A}
E Greenland	body feathers	10	1.47±0.58 ^{A,B}	9	0.33±0.13 ^{A,B}	1.41±0.22 ^{A,B}	-0.01±0.12 ^{A}	1.18±0.06 ^{A}
Spitsbergen	body feathers	10	1.06±0.41 ^{A,B}	9	0.22±0.22 ^{A}	1.27±0.18 ^{A}	-0.03±0.01 ^{A}	1.13±0.09 ^{A}
NW Greenland	body feathers	10	2.07±0.52 ^{C}	10	0.57±0.20 ^{C}	1.23±0.16 ^{A}	0.01±0.04 ^{A}	1.21±0.10 ^{A}

Table S5. Carbon ($\delta^{13}C$, proxy of foraging habitat) and nitrogen ($\delta^{15}N$ trophic position) isotopic values (Mean ± SD, ‰) of head and body feathers and blood samples of little auks. Values not sharing the same superscript letter within each group are statistically different.

Population	n	Head feather $\delta^{13}C$ (‰)	Body feather $\delta^{13}C$ (‰)	Blood $\delta^{13}C$ (‰)	Head feather $\delta^{15}N$ (‰)	Body feather $\delta^{15}N$ (‰)	Blood $\delta^{15}N$ (‰)
FJL	10	-20.59±0.40^{A}	-21.53±0.40^{B}	-23.13±0.84^{B,C}	14.41±0.50^{D}	14.57±0.38^{A}	11.70±0.09^{A,B}
Bear Island	10	-20.35±0.38^{A}	-20.87±0.11^{B}	-21.57±0.22^{B}	13.45±10.97^{C}	14.50±0.21^{A,B}	11.12±0.32^{A}
East Greenland	10	-19.61±0.46^{B}	-20.67±0.46^{A}	-22.09±0.47^{B}	11.27±1.15^{A}	13.10±0.61^{B}	11.81±0.17^{A,B}
Spitsbergen	10	-20.25±0.26^{A}	-21.12±0.56^{B}	-21.12±0.19^{B}	13.24±0.69^{B,C}	14.18±0.48^{A,B}	11.36±0.33^{A}
NW Greenland	10	-19.41±0.57^{B}	-19.87±0.42^{B}	-20.07±0.35^{A}	12.41±0.95^{A,B}	14.47±1.09^{A}	12.28±0.14^{B}

Table S6. Linear mixed models (LMM) and Linear regression (Lineal-Model Pearson) for statistical correlations of body feather total Hg concentration ($\mu g \cdot g^{-1}$) and Hg isotopic values ($\delta^{202}Hg$, $\Delta^{199}Hg$ and $\Delta^{200}Hg$) with summer latitude, summer longitude and both variables together as predictors. Models are ranked by ΔAICc with the degrees of freedom (df), Akaike weights (wi), and marginal R^2.

Statistical test	Mixed models						Linear regression (Linear Model-Spearman)			
Variable	**Predictors**	**df**	**AICc**	**ΔAICc**	**wi**	**R^2m**	**Slope**	**Intercept**	**R^2 (Adjusted)**	**p**
Body feather THg	~ **Summer longitude**	3	59.996	0.000	1.000	0.565	-0.012	1.209	0.573	**< 0.0001**
Body feather THg	**~ Summer latitude + Summer longitude**	4	60.516	0.52	0.771	0.435			0.253	**< 0.0001**
Body feather THg	~ **Summer latitude**	3	102.583	42.587	0.000	0.000	-0.027	3.299	0.002	0.3409
Body feather $\delta^{202}Hg$	~ **Summer latitude**	3	20.017	0.000	1.000	0.621	0.052	-3.421	0.247	**< 0.0001**
Body feather $\delta^{202}Hg$	**~ Summer latitude + Summer longitude**	4	21.032	1.015	0.602	0.374			0.253	**0.0007**
Body feather $\delta^{202}Hg$	~ **Summer longitude**	3	29.386	9.369	0.009	0.006	0.002	0.543	0.077	0.034
Body feather $\Delta^{199}Hg$	~ **Summer longitude**	3	-7.577	0.000	1.000	0.758	0.003	1.385	0.204	**< 0.0001**
Body feather $\Delta^{199}Hg$	**~ Summer latitude + Summer longitude**	4	-5.243	2.334	0.311	0.236			0.253	**< 0.0001**
Body feather $\Delta^{199}Hg$	~ **Summer latitude**	3	2.213	9.79	0.007	0.006	0.014	0.319	0.015	0.203
Body feather $\Delta^{200}Hg$	~ **Summer longitude**	3	-102.14	0.000	1.000	0.535	0.000	-0.007	0.003	0.291
Body feather $\Delta^{200}Hg$	~ **Summer latitude**	3	-100.993	1.147	0.564	0.301	-0.001	0.040	0.022	0.863
Body feather $\Delta^{200}Hg$	**~ Summer latitude + Summer longitude**	4	-99.776	2.364	0.307	0.164			0.253	< 0.0001

Table S7. Linear mixed models (LMM) and Linear regression (lineal-Model Pearson) for statistical correlations of head feather total Hg concentration (μg·g^{-1}) and Hg isotopic values (δ^{202}Hg. Δ^{199}Hg and Δ^{200}Hg) with median winter latitude. median winter longitude and both variables together. Models are ranked by ΔAICc with the degrees of freedom (df), Akaike weights (wi), and marginal R^2.

Statistical test	Linear Mixed Models						Linear regression (Linear Model)			
Variable	**Predictors**	**df**	**AICc**	**ΔAICc**	**wi**	**R^2m**	**Slope**	**Intercept**	**R^2 (Adjusted)**	**p**
Head feather THg	**~ Winter latitude + Winter longitude**	4	90.021	0.000	1.000	0.442			0.440	**< 0.0001**
Head feather THg	~ **Winter longitude**	3	90.132	0.111	0.946	0.418	-0.022	2.287	0.417	**< 0.0001**
Head feather THg	~ **Winter latitude**	3	92.236	2.305	0.316	0.140	-0.050	5.718	0.382	**< 0.0001**
Head feather δ^{202}Hg	**~ Winter latitude + Winter longitude**	4	6.207	0.000	1.000	0.600			0.640	**< 0.0001**
Head feather δ^{202}Hg	~ **Winter longitude**	3	7.034	0.827	0.661	0.397	0.010	0.644	0.618	**< 0.0001**
Head feather δ^{202}Hg	~ **Winter latitude**	3	16.58	10.373	0.006	0.003	0.024	-0.948	0.505	**< 0.0001**
Head feather Δ^{199}Hg	~ **Winter longitude**	3	-48.524	0.000	1.000	0.716	0.002	1.069	0.218	**< 0.0001**
Head feather Δ^{199}Hg	**~ Winter latitude + Winter longitude**	4	-46.459	2.065	0.356	0.255			0.205	**0.007**
Head feather Δ^{199}Hg	~ **Winter latitude**	3	-42.144	6.38	0.041	0.029	0.003	0.833	0.071	0.061
Head feather Δ^{200}Hg	~ **Winter latitude**	3	-110.754	0.000	1.000	0.676	-0.002	0.095	0.130	**0.016**
Head feather Δ^{200}Hg	**~ Winter latitude + Winter longitude**	4	-108.646	2.108	0.349	0.236			0.115	**0.048**
Head feather Δ^{200}Hg	~ **Winter longitude**	3	-106.677	4.077	0.13	0.088	0.000	-0.017	0.029	0.158

Table S8. Differences between head and body feather for: A) total Hg (THg) concentrations (μg·g^{-1}, dw) B) δ^{202}Hg; C) Δ^{199}Hg and C) Δ^{200}Hg values (‰). Associated statistics correspond to randomization procedures with a confidence interval (CI) of 99%.

A)		Head feathers THg (μg·g^{-1})	Body feathers THg (μg·g^{-1})	Diff THg head-body feathers (μg·g^{-1})	Randomization test			
Population	n	Mean ± SD	Mean ± SD	Mean ± SD	Observed diff	Randon mean	Random CI left	Random CI right
FJL	9	1.74±0.54	0.75±0.12	0.82±0.77	0.982	0.983	0.997	0.969
Bear Island	10	2.65±1.15	0.71±0.18	1.94±1.17	1.911	1.897	1.932	1.862
East Greenland	10	3.48±0.58	1.47±0.58	2.01±0.84	1.968	1.962	1.983	1.940
Spitsbergen	9	2.69±0.72	1.06±0.41	1.62±1.03	1.542	1.542	1.565	1.518
NW Greenland	10	2.15±0.40	2.07±0.52	0.08±0.68	0.077	0.069	0.085	0.053

B)		Head feathers δ^{202}Hg (‰)	Body feathers δ^{202}Hg (‰)	Diff δ^{202}Hg head-body feathers (‰)	Randomization test			
Population	n	Mean ± SD	Mean ± SD	Mean ± SD	Observed diff	Randon mean	Random CI left	Random CI right
FJL	9	0.94±0.30	0.96±0.21	-0.03±0.30	-0.025	-0.022	-0.013	-0.032
Bear Island	10	0.53±0.25	0.57±0.28	0.07±0.37	-0.021	-0.024	-0.013	-0.034
East Greenland	10	0.10±0.20	0.33±0.13	-0.20±0.28	-0.233	-0.231	-0.224	-0.237
Spitsbergen	9	0.40±0.33	0.22±0.22	0.16±0.43	0.149	0.151	0.161	0.142
NW Greenland	10	0.80±0.21	0.57±0.20	0.23±0.29	0.230	0.229	0.236	0.222

C)		Head feathers Δ^{199}Hg (‰)	Body feathers Δ^{199}Hg (‰)	Diff Δ^{199}Hg head-body feathers (‰)	Randomization test			
Population	n	Mean ± SD	Mean ± SD	Mean ± SD	Observed diff	Randon mean	Random CI left	Random CI right
FJL	9	1.54±0.11	1.80±0.14	-0.51 ±0.12	-0.506	-0.504	-0.499	-0.508
Bear Island	10	1.13±0.11	1.26±0.11	-0.02±0.59	-0.284	-0.287	0.280	-0.294
East Greenland	10	1.41±0.06	1.51±0.12	-0.27±0.55	-0.426	-0.426	-0.419	-0.433
Spitsbergen	9	1.60±0.04	1.82±0.09	-0.29±0.60	-0.329	-0.327	-0.320	-0.333
NW Greenland	10	1.54±0.06	1.86±0.08	-0.26±0.19	-0.256	-0.257	-0.252	-0.261

D)		Head feathers Δ^{200}Hg (‰)	Body feathers Δ^{200}Hg (‰)	Diff Δ^{200}Hg head-body feathers (‰)	Randomization test			
Population	n	Mean ± SD	Mean ± SD	Mean ± SD	Observed diff	Randon mean	Random CI left	Random CI right
FJL	9	-0.03±0.05	-0.02±0.05	-0.01±0.06	-0.009	-0.009	-0.007	-0.011
Bear Island	10	0.01±0.05	0.00±0.04	0.01±0.06	-0.003	-0.002	-0.001	-0.003
East Greenland	10	0.02±0.06	-0.01±0.12	0.03±0.14	0.040	0.041	0.044	0.037
Spitsbergen	9	-0.05±0.04	-0.03±0.01	-0.02±0.13	-0.031	-0.032	-0.029	-0.035
NW Greenland	10	-0.02±0.01	0.01±0.04	-0.04±0.07	-0.041	-0.039	-0.038	-0.041

Table S9. Total Hg concentrations (μg·g^{-1}, dw), Hg isotopic composition and carbon and nitrogen isotopic values of body feathers of little auks.

Individual	**Year**	**Site**	**Hg**	**δ^{204}Hg**	**δ^{202}Hg**	**δ^{201}Hg**	**δ^{200}Hg**	**δ^{199}Hg**	**Δ^{204}Hg**	**Δ^{201}Hg**	**Δ^{200}Hg**	**Δ^{199}Hg**	**δ^{13}C**	**δ^{15}N**

			(µg·g^{-1})	(‰)	(‰)	(‰)	(‰)	(‰)	(‰)	(‰)	(‰)	(‰)	(‰)	(‰)
DA29201	2015	Bear Island	0.89	1.00	0.64	1.33	0.30	1.13	0.04	0.85	-0.02	0.97	NA	NA
DA42341	2015	Bear Island	0.94	0.71	0.46	1.06	0.15	1.28	0.02	0.71	-0.08	1.16	NA	NA
DA47406	2015	Bear Island	0.40	NA	NA	NA	NA	NA	NA	NA	NA	NA	NA	NA
DA47408	2015	Bear Island	0.69	1.12	0.79	1.68	0.43	1.71	-0.06	1.08	0.03	1.51	NA	NA
DA47409	2015	Bear Island	0.60	NA	NA	NA	NA	NA	NA	NA	NA	NA	NA	NA
DA47414	2015	Bear Island	0.56	0.29	0.23	1.69	0.17	1.77	-0.06	1.52	0.05	1.71	NA	NA
DA47415	2015	Bear Island	0.62	1.43	0.93	1.88	0.47	1.52	0.04	1.17	0.00	1.28	NA	NA
DA47419	2015	Bear Island	0.66	1.28	0.88	1.85	0.44	1.62	-0.03	1.19	0.00	1.40	NA	NA
DA47371	2016	Bear Island	0.92	0.53	0.34	1.48	0.19	1.59	0.02	1.22	0.02	1.50	-20.79	14.35
DA47373	2016	Bear Island	0.87	0.45	0.29	1.36	0.17	1.26	0.02	1.14	0.03	1.19	-20.95	14.64
HS012833	2015	FJL	0.76	1.40	0.94	1.85	0.47	1.68	0.00	1.14	-0.01	1.44	-21.88	14.82
HS012817	2015	FJL	0.79	1.19	0.78	1.99	0.39	1.92	0.04	1.41	0.00	1.72	-21.73	14.66
HS012818	2015	FJL	0.99	1.70	1.15	2.28	0.52	1.94	-0.02	1.41	-0.05	1.65	-21.48	15.02
HS012822	2015	FJL	0.75	1.60	1.02	2.09	0.46	1.72	0.08	1.32	-0.05	1.46	-21.55	14.49
HS012834	2015	FJL	0.74	1.49	0.91	2.40	0.51	2.14	0.13	1.72	0.05	1.91	-21.52	14.2
HS012839	2015	FJL	0.83	2.02	1.28	2.43	0.66	2.00	0.12	1.47	0.02	1.68	-21.84	14.56
HS012828	2015	FJL	0.73	1.34	0.89	2.10	0.45	1.87	0.01	1.44	0.01	1.65	-21.72	14.43
HS012829	2015	FJL	0.50	1.71	1.26	2.19	0.61	1.82	-0.17	1.24	-0.02	1.50	-21.37	14.13
HS012604	2016	FJL	0.76	1.12	0.69	2.09	0.34	1.98	0.09	1.58	-0.01	1.81	-21.21	14.50
HS012606	2016	FJL	0.68	0.87	0.69	1.95	0.24	1.75	-0.17	1.42	-0.11	1.58	-21.00	14.89
DA50219	2016	Spitsbergen	1.44	0.20	0.05	1.20	0.03	1.43	0.13	1.16	0.00	1.41	-20.55	13.87
DA50220	2016	Spitsbergen	1.92	0.27	0.07	1.08	0.01	1.21	0.17	1.02	-0.03	1.19	-20.99	13.66
DA50221	2016	Spitsbergen	0.77	0.34	0.22	1.46	-0.02	1.42	0.01	1.29	-0.13	1.36	-20.56	13.84
DA50224	2016	Spitsbergen	1.30	0.55	0.24	1.11	-0.03	0.97	0.19	0.93	-0.16	0.90	-20.58	13.46
DA50227	2016	Spitsbergen	0.70	0.59	0.52	1.62	0.11	1.41	-0.18	1.23	-0.15	1.28	-21.65	14.6
DA50229	2016	Spitsbergen	0.88	-0.12	-0.11	1.15	0.08	1.39	0.05	1.24	0.14	1.42	-21.39	14.49
DA50230	2016	Spitsbergen	0.82	0.04	0.09	1.11	0.09	1.30	-0.10	1.04	0.05	1.28	-21.21	14.54

DA50234	2016	Spitsbergen	0.69	NA	NA	NA	NA	NA	NA	NA	NA	NA	-22.31	14.42
DA50235	2016	Spitsbergen	0.79	0.44	0.41	1.63	0.22	1.61	-0.18	1.32	0.01	1.51	-21.18	14.95
DA50239	2016	Spitsbergen	1.35	0.77	0.49	1.27	0.25	1.24	0.04	0.90	0.01	1.12	-20.77	13.99
LIAK15EG01	2015	East Greenland	1.42	0.26	0.19	1.26	0.07	1.35	-0.02	1.11	-0.03	1.30	-21.29	13.49
LIAK15EG02	2015	East Greenland	1.06	0.53	0.38	1.64	0.14	1.61	-0.03	1.36	-0.05	1.51	-21.26	13.47
LIAK15EG03	2015	East Greenland	1.07	0.42	0.34	1.82	-0.06	1.89	-0.08	1.57	-0.23	1.80	-20.3	13.09
LIAK15EG04	2015	East Greenland	1.20	0.74	0.52	1.64	0.41	1.64	-0.02	1.25	0.15	1.51	-20.24	12.78
LIAK15EG05	2015	East Greenland	1.03	0.69	0.36	1.55	0.16	1.56	0.16	1.28	-0.02	1.47	-20.47	13.54
LAIK15EG10	2015	East Greenland	2.32	NA	NA	NA	NA	NA	NA	NA	NA	NA	-20.71	11.57
LIAK15EG36	2015	East Greenland	2.75	0.69	0.43	1.36	0.12	1.24	0.04	1.04	-0.10	1.13	-19.89	13.45
LIAK15EG37	2015	East Greenland	1.39	0.71	0.42	1.50	0.25	1.59	1.54	1.18	0.04	1.49	-21	13.34
LIAK16EG02	2016	East Greenland	1.22	0.04	0.13	1.25	0.05	1.47	-0.14	1.16	-0.01	1.44	-20.6	12.77
LIAK16EG06	2016	East Greenland	1.24	0.21	0.23	1.01	0.28	1.13	-0.13	0.84	0.17	1.07	-20.94	13.46
51676	2016	NW Greenland	1.69	0.77	0.53	1.35	0.20	1.22	-0.01	0.95	-0.07	1.09	-20.44	15.05
51679	2016	NW Greenland	2.40	0.41	0.27	1.29	0.15	1.36	0.01	1.08	0.01	1.30	-19.79	16.08
51681	2016	NW Greenland	1.32	0.68	0.44	1.42	0.27	1.47	0.03	1.10	0.05	1.36	-20.48	14.05
51683	2016	NW Greenland	1.81	1.34	0.94	1.74	0.57	1.49	-0.06	1.04	0.10	1.26	-19.38	14.15
51684	2016	NW Greenland	1.82	1.08	0.66	1.83	0.38	1.68	0.09	1.33	0.04	1.51	-19.37	12.98
51685	2016	NW Greenland	2.04	1.10	0.78	1.67	0.39	1.57	-0.07	1.08	0.00	1.37	-20.2	13.64
51686	2016	NW Greenland	2.07	0.69	0.44	1.34	0.21	1.24	0.04	1.01	-0.01	1.13	-19.48	14.5
51689	2016	NW Greenland	3.28	1.06	0.64	1.35	0.33	1.14	0.11	0.87	0.00	0.98	-20.19	15.97
51692	2016	NW Greenland	2.16	0.59	0.40	1.07	0.21	1.22	0.00	0.77	0.01	1.12	-19.77	15.21
51693	2016	NW Greenland	2.16	1.09	0.59	1.35	0.35	1.25	0.21	0.91	0.05	1.11	-19.64	13.11

Table S10. Winter distribution (median latitude and longitude coordinates) of little auks, total Hg concentrations (μg·g^{-1}, dw), Hg isotopic composition and carbon and nitrogen isotopic values of head feathers.

Individual	**Year**	**Site**	**Median latitude winter**	**Median longitude winter**	**Hg (μg·g^{-1})**	**δ^{204}Hg (‰)**	**δ^{202}Hg (‰)**	**δ^{201}Hg (‰)**	**δ^{200}Hg (‰)**	**δ^{199}Hg (‰)**	**Δ^{204}Hg (‰)**	**Δ^{201}Hg (‰)**	**Δ^{200}Hg (‰)**	**Δ^{199}Hg (‰)**	**δ^{13}C (‰)**	**δ^{15}N (‰)**

DA29201	2015	Bear Island	68.91	-10.83	2.35	0.74	0.57	1.32	0.30	1.27	-0.10	0.90	0.02	1.13	-20.87	13.17
DA42341	2015	Bear Island	61.52	-42.78	3.56	0.62	0.36	1.10	0.19	1.04	0.08	0.83	0.00	0.94	-20.60	14.11
DA47406	2015	Bear Island	64.18	-38.17	4.35	0.39	0.39	1.22	0.23	1.20	-0.19	0.93	0.03	1.10	-20.76	13.96
DA47408	2015	Bear Island	68.47	-11.97	2.65	0.60	0.34	1.34	0.22	1.22	0.09	1.08	0.05	1.14	-20.74	14.43
DA47409	2015	Bear Island	51.42	-47.19	2.71	0.79	0.52	1.18	0.33	1.08	0.01	0.79	0.07	0.94	-19.97	11.28
DA47414	2015	Bear Island	68.17	-4.49	0.81	1.23	0.78	1.69	0.31	1.46	0.06	1.10	-0.08	1.26	-20.36	13.79
DA47415	2015	Bear Island	69.55	-6.33	1.04	1.57	1.14	1.78	0.55	1.44	-0.14	0.92	-0.02	1.15	-19.97	13.85
DA47419	2015	Bear Island	59.23	-43.61	3.89	0.70	0.38	1.01	0.19	0.98	0.14	0.73	0.00	0.89	-19.80	12.24
DA47371	2016	Bear Island	NA	NA	2.09	0.68	0.43	1.16	0.19	1.10	0.03	0.83	-0.03	0.99	-20.09	13.90
DA47373	2016	Bear Island	68.67	-10.95	3.06	0.53	0.38	0.94	0.26	1.04	-0.05	0.65	0.07	0.94	-20.39	13.74
HS012833	2015	FJL	70.82	53.40	1.19	1.26	0.63	1.45	0.29	1.21	0.31	0.97	-0.03	1.06	-20.61	14.20
HS012817	2015	FJL	75.67	51.94	1.19	1.75	1.07	1.92	0.54	1.42	0.15	1.12	0.00	1.15	-20.15	14.46
HS012818	2015	FJL	76.56	48.49	2.28	1.57	1.07	1.82	0.51	1.40	-0.03	1.01	-0.02	1.13	-20.07	15.58
HS012822	2015	FJL	75.44	-1.05	1.91	0.60	0.47	1.19	0.10	1.16	-0.11	0.83	-0.14	1.05	-21.16	13.99
HS012834	2015	FJL	76.07	47.66	1.82	1.60	1.08	1.83	0.52	1.52	-0.01	1.02	-0.02	1.24	-20.66	14.34
HS012839	2015	FJL	76.05	54.77	1.89	1.39	1.03	1.55	0.48	1.36	-0.16	0.78	-0.04	1.10	-21.00	14.28
HS012828	2015	FJL	73.80	12.28	1.50	NA	NA	NA	NA	NA	NA	NA	NA	NA	-21.01	13.92
HS012829	2015	FJL	77.14	41.12	1.04	2.15	1.43	1.96	0.66	1.47	0.02	0.89	-0.06	1.11	-20.08	14.96
HS012604	2016	FJL	75.84	31.01	1.31	1.65	1.04	1.87	0.54	1.42	0.10	1.09	0.02	1.16	-20.40	14.18
HS012606	2016	FJL	74.14	2.09	2.73	1.08	0.66	1.50	0.34	1.36	0.10	1.01	0.01	1.20	-20.71	14.17
DA50219	2016	Spitsbergen	67.93	-10.49	1.67	0.97	0.65	1.28	0.29	1.13	-0.01	0.79	-0.04	0.96	-19.84	13.09
DA50220	2016	Spitsbergen	67.10	-5.89	2.25	1.13	0.65	1.41	0.31	1.37	0.16	0.92	-0.02	1.20	-20.60	12.83
DA50221	2016	Spitsbergen	61.95	-53.02	3.79	0.51	0.33	0.99	0.19	1.02	0.01	0.74	0.02	0.93	-20.00	12.50
DA50224	2016	Spitsbergen	67.89	-11.22	2.10	0.48	0.25	0.87	0.11	0.87	0.11	0.68	-0.01	0.80	-20.34	13.30
DA50227	2016	Spitsbergen	71.06	4.38	2.58	NA	NA	NA	NA	NA	NA	NA	NA	NA	-20.21	14.48
DA50229	2016	Spitsbergen	67.35	-8.87	2.74	0.29	0.01	0.77	-0.06	0.84	0.28	0.76	-0.06	0.84	-20.27	12.46
DA50230	2016	Spitsbergen	61.29	-41.35	3.63	-0.34	-0.15	0.52	-0.18	0.85	-0.12	0.64	-0.10	0.89	-19.94	12.60
DA50234	2016	Spitsbergen	70.03	-9.06	3.52	1.39	0.93	1.63	0.40	1.30	0.00	0.93	-0.07	1.06	-20.54	13.77
DA50235	2016	Spitsbergen	68.93	-8.89	2.32	0.76	0.47	1.06	0.18	0.97	0.06	0.70	-0.05	0.85	-20.32	13.52

DA50239	2016	Spitsbergen	73.24	-3.52	2.34	0.46	0.44	1.13	0.13	1.18	-0.19	0.80	-0.09	1.07	-20.47	13.84
LIAK15EG01	2015	East Greenland	46.62	-45.35	3.59	-0.05	-0.05	0.92	0.09	1.24	0.02	0.96	0.12	1.25	-19.40	9.96
LIAK15EG02	2015	East Greenland	45.72	-46.50	2.63	0.55	0.37	0.92	0.18	1.04	0.00	0.64	0.00	0.94	-19.34	11.86
LIAK15EG03	2015	East Greenland	45.08	-47.84	3.63	0.15	0.23	0.95	0.16	1.09	-0.19	0.78	0.04	1.03	-19.50	11.16
LIAK15EG04	2015	East Greenland	45.67	-43.43	3.69	0.07	0.02	0.83	-0.01	1.00	0.03	0.82	-0.02	0.99	-19.34	10.26
LIAK15EG05	2015	East Greenland	47.49	-40.60	4.32	-0.27	-0.16	0.67	-0.01	1.10	-0.03	0.79	0.07	1.14	-19.71	10.10
LAIK15EG10	2015	East Greenland	46.49	-42.32	4.33	-0.07	0.16	1.17	0.01	1.17	-0.31	1.05	-0.07	1.13	-20.14	10.09
LIAK15EG36	2015	East Greenland	51.16	-50.06	2.83	0.30	0.32	1.05	0.23	1.11	-0.18	0.81	0.07	1.02	-19.39	11.75
LIAK15EG37	2015	East Greenland	46.64	-45.25	3.15	-0.33	-0.24	0.44	-0.12	0.66	0.03	0.62	0.00	0.72	-18.84	11.94
LIAK16EG02	2016	East Greenland	NA	NA	3.01	0.42	0.21	0.97	0.08	0.97	0.10	0.81	-0.02	0.92	-20.16	12.07
LIAK16EG06	2016	East Greenland	40.16	-46.47	3.60	0.10	0.17	0.92	0.11	0.91	-0.16	0.79	0.02	0.87	-20.30	13.46
51676	2016	NW Greenland	NA	NA	2.36	1.38	0.88	1.47	0.41	1.17	0.07	0.81	-0.03	0.95	-18.98	13.57
51679	2016	NW Greenland	NA	NA	2.59	1.52	0.94	1.52	0.45	1.42	0.12	0.82	-0.02	1.19	-19.98	12.05
51681	2016	NW Greenland	NA	NA	2.58	1.04	0.74	1.40	0.44	1.14	-0.07	0.84	0.07	0.95	-20.19	10.98
51683	2016	NW Greenland	NA	NA	1.49	1.28	0.94	1.45	0.38	1.14	-0.13	0.74	-0.09	0.90	-18.78	12.67
51684	2016	NW Greenland	NA	NA	2.47	0.42	0.28	0.88	0.16	0.98	0.01	0.67	0.02	0.91	-19.94	10.71
51685	2016	NW Greenland	NA	NA	1.70	1.15	0.86	1.44	0.40	1.15	-0.14	0.79	-0.03	0.93	-19.53	12.19
51686	2016	NW Greenland	NA	NA	2.44	1.47	0.93	1.51	0.42	1.20	0.08	0.81	-0.05	0.97	-19.26	12.91
51689	2016	NW Greenland	NA	NA	2.20	1.80	0.97	1.55	0.51	1.26	0.36	0.82	0.02	1.01	-19.66	13.25
51692	2016	NW Greenland	NA	NA	1.81	1.08	0.72	1.25	0.26	1.04	0.01	0.71	-0.10	0.86	-18.41	13.22
51693	2016	NW Greenland	NA	NA	1.87	1.00	0.72	1.42	0.37	1.16	-0.08	0.88	0.00	0.98	-19.33	12.53

Table S11. Total Hg concentrations (μg·g^{-1}, dw), Hg isotopic composition and carbon and nitrogen isotopic values of blood samples of little auks.

Individual	Year	Site	Hg (μg·g^{-1})	δ^{204}Hg (‰)	δ^{202}Hg (‰)	δ^{201}Hg (‰)	δ^{200}Hg (‰)	δ^{199}Hg (‰)	Δ^{204}Hg (‰)	Δ^{201}Hg (‰)	Δ^{200}Hg (‰)	Δ^{199}Hg (‰)	δ^{13}C (‰)	δ^{15}N (‰)
DA29201	2015	Bear Island	0.52	1.83	1.27	2.20	0.69	1.73	-0.07	1.24	0.05	1.41	-21.62	11.26
DA42341	2015	Bear Island	0.38	1.98	1.30	2.13	0.65	1.74	0.04	1.15	0.00	1.41	-21.42	11.16
DA47406	2015	Bear Island	0.53	1.91	1.41	2.17	0.65	1.77	-0.19	1.12	-0.05	1.42	-21.82	10.50
DA47408	2015	Bear Island	0.45	1.81	1.26	2.15	0.63	1.67	-0.07	1.20	0.00	1.36	-21.54	10.88
DA47409	2015	Bear Island	0.35	1.52	1.03	1.93	0.56	1.60	-0.02	1.15	0.04	1.34	-21.40	10.77
DA47414	2015	Bear Island	0.26	1.46	1.15	2.26	0.56	1.94	-0.26	1.39	-0.02	1.65	-21.31	11.37
DA47415	2015	Bear Island	0.50	2.26	1.55	2.46	0.82	1.86	-0.05	1.30	0.04	1.47	-21.58	11.33
DA47419	2015	Bear Island	NA	1.22	0.79	1.59	0.37	1.31	0.04	0.99	-0.03	1.11	-21.28	11.59
DA47371	2016	Bear Island	0.30	1.89	1.29	2.03	0.62	1.60	-0.03	1.06	-0.03	1.27	-21.96	11.04
DA47373	2016	Bear Island	0.41	2.06	1.58	2.31	0.76	1.73	-0.29	1.13	-0.03	1.33	-21.73	11.25
HS012833	2015	FJL	0.38	2.25	1.45	2.53	0.73	2.13	0.09	1.43	0.00	1.76	-22.95	11.71
HS012817	2015	FJL	0.27	NA	NA	NA	NA	NA	NA	NA	NA	NA	-23.48	11.73
HS012818	2015	FJL	0.53	2.69	1.77	2.74	0.93	2.10	0.05	1.41	0.04	1.65	-22.88	11.85
HS012822	2015	FJL	0.29	2.11	1.52	2.59	0.77	1.98	-0.16	1.44	0.01	1.60	-23.32	11.78
HS012834	2015	FJL	0.29	NA	NA	NA	NA	NA	NA	NA	NA	NA	-23.49	11.75
HS012839	2015	FJL	0.33	2.32	1.50	2.82	0.81	2.34	0.08	1.69	0.05	1.96	-24.37	11.58
HS012828	2015	FJL	0.22	2.10	1.34	2.79	0.58	2.27	0.09	1.78	-0.09	1.93	-23.90	11.55
HS012829	2015	FJL	0.22	NA	NA	NA	NA	NA	NA	NA	NA	NA	-23.36	11.61
HS012604	2016	FJL	0.29	1.82	1.23	2.52	0.57	2.20	-0.01	1.60	-0.04	1.89	-21.66	11.67
HS012606	2016	FJL	0.22	NA	NA	NA	NA	NA	NA	NA	NA	NA	-21.85	11.72

Supplementary discussion: geographical patterns of even-MIF signatures (Δ^{200}Hg)

Hg even-MIF (Δ^{200}Hg) of body feathers ranged widely (-0.23 to 0.17‰) whereas less variability was observed for head feathers (-0.14 to 0.12‰). No significant inter-population differences in Δ^{200}Hg values of body feathers ($H=3.685$, $p=0.45$) seem to indicate similar atmospheric sources in all the studied breeding colonies in summer. Body feather Δ^{200}Hg values were not linearly related neither to latitude ($p=0.83$) nor longitude ($p=0.27$) (Fig. S5). No trend was neither observed for head feather Δ^{200}Hg values with winter longitude ($p=0.15$). However, Δ^{200}Hg values of head feathers were negatively and significantly related to winter latitude ($R^2=0.13$, $p=0.016$), decreasing from East Greenland (0.02 ± 0.06‰) to Spitsbergen (-0.05 ± 0.04‰) individuals. Atmospheric and riverine inputs are believed to be the major drivers of Hg originating from industrialized countries [5]. The occurrence of atmospheric Hg depletion events (AMDEs) in the Arctic has been considered to drive significant deposition of atmospheric Hg from mid-latitude anthropogenic emissions into sea ice [6]. Although we could suppose a relative contribution of Hg released from snow in seabirds wintering in Arctic northern regions, Δ^{200}Hg values in feathers were in general more positive than those previously documented in Arctic snow impacted by AMDEs (-0.12‰ [7]). Recent modelling studies estimated limited uptake of Hg^0 in the Arctic Ocean as a result of ice cover and saturation of surface waters in dissolved Hg^0 [8]. Arctic tundra and vegetation also seem to play an important role in the uptake of atmospheric Hg and in its transfer to boreal soils [9], later mobilized to the ocean by snowmelt and river circulation. Recent works also reconsidered Arctic river Hg fluxes

as important contributors of Hg from continental inputs towards the Arctic Ocean [8,10]. The low Δ^{200}Hg values observed in boreal soils (−0.02 ± 0.03‰ [9]) and Arctic Ocean sediments (0.00 ± 0.03‰ [11]) match the close-to-zero mean Δ^{200}Hg values registered in feathers of little auks of northern regions. This could suggest a predominance of continental and riverine inputs over the Arctic and North Atlantic Oceans as suggested by recent observations [8,10]. However, the high degree of intra-population uncertainty does not allow us to make conclusive deductions about the contribution of atmospheric, sea ice melting or continental Hg inputs across the wintering sites of little auks.

References

(1) Bergquist, B. A.; Blum, J. D. Mass-Dependent and -Independent Fractionation of Hg Isotopes by Photoreduction in Aquatic Systems. *Science* **2007**, *318* (5849), 417–420. https://doi.org/10.1126/science.1148050.

(2) Renedo, M.; Bustamante, P.; Tessier, E.; Pedrero, Z.; Cherel, Y.; Amouroux, D. Assessment of Mercury Speciation in Feathers Using Species-Specific Isotope Dilution Analysis. *Talanta* **2017**, *174*. https://doi.org/10.1016/j.talanta.2017.05.081.

(3) Renedo, M.; Amouroux, D.; Duval, B.; Carravieri, A.; Tessier, E.; Barre, J.; Bérail, S.; Pedrero, Z.; Cherel, Y.; Bustamante, P. Seabird Tissues As Efficient Biomonitoring Tools for Hg Isotopic Investigations: Implications of Using Blood and Feathers from Chicks and Adults. *Environ. Sci. Technol.* **2018**, *52* (7), 4227–4234. https://doi.org/10.1021/acs.est.8b00422.

(4) Yamakawa, A.; Takeuchi, A.; Shibata, Y.; Berail, S.; Donard, O. F. X. Determination of Hg Isotopic Compositions in Certified Reference Material NIES No. 13 Human Hair by Cold Vapor Generation Multi-Collector Inductively Coupled Plasma Mass Spectrometry. *Accredit. Qual. Assur.* **2016**, No. 13. https://doi.org/10.1007/s00769-016-1196-x.

(5) Kirk, J. L.; Lehnherr, I.; Andersson, M.; Braune, B. M.; Chan, L.; Dastoor, A. P.; Durnford, D.; Gleason, A. L.; Loseto, L. L.; Steffen, A.; St. Louis, V. L. Mercury in Arctic Marine Ecosystems: Sources, Pathways and Exposure. *Environ. Res.* **2012**, *119*, 64–87. https://doi.org/10.1016/j.envres.2012.08.012.

(6) Larose, C.; Dommergue, A.; Marusczak, N.; Coves, J.; Ferrari, C. P.; Schneider, D. Bioavailable Mercury Cycling in Polar Snowpacks. *Environ. Sci. Technol.* **2011**, *45*, 2150–2156. https://doi.org/10.1021/es103016x.

(7) Sherman, L. S.; Blum, J. D.; Johnson, K. P.; Keeler, G. J.; Barres, J. a.; Douglas, T. a. Mass-Independent Fractionation of Mercury Isotopes in Arctic Snow Driven by Sunlight. *Nat. Geosci.* **2010**, *3* (3), 173–177. https://doi.org/10.1038/ngeo758.

(8) Soerensen, A. L.; Jacob, D. J.; Schartup, A. T.; Fisher, J. A.; Lehnherr, I.; Louis, V. L. S.; Heimbürger, L.; Sonke, J. E.; Krabbenhoft, D. P.; Sunderland, E. M. A Mass Budget for Mercury and Methylmercury in the Arctic Ocean. *Global Biogeochem. Cycles* **2016**, No. 30, 560–575. https://doi.org/10.1002/2015GB005280.Received.

(9) Obrist, D.; Agnan, Y.; Jiskra, M.; Olson, C. L.; Dominique, P.; Hueber, J.; Moore, C. W.; Sonke, J.; Helmig, D. Tundra Uptake of Atmospheric Elemental Mercury Drives Arctic Mercury Pollution. *Nat. Publ. Gr.* **2017**, *547* (7662), 201–204. https://doi.org/10.1038/nature22997.

(10) Sonke, J. E.; Teisserenc, R.; Heimbürger-Boavida, L.-E.; Petrova, M. V.;

Marusczak, N.; Le Dantec, T.; Chupakov, A. V.; Li, C.; Thackray, C. P.; Sunderland, E. M.; Tananaev, N.; Pokrovsky, O. S. Eurasian River Spring Flood Observations Support Net Arctic Ocean Mercury Export to the Atmosphere and Atlantic Ocean. *Proc. Natl. Acad. Sci.* **2018**, 201811957. https://doi.org/10.1073/pnas.1811957115.

(11) Gleason, J. D.; Blum, J. D.; Moore, T. C.; Polyak, L.; Jakobsson, M.; Meyers, P. A.; Biswas, A. Sources and Cycling of Mercury in the Paleo Arctic Ocean from Hg Stable Isotope Variations in Eocene and Quaternary Sediments. *Geochim. Cosmochim. Acta* **2016**, *197* (245–262). https://doi.org/10.1016/j.gca.2016.10.033.